Excitation of surface plasmon-polaritons in metal films with double periodic modulation: Anomalous optical effects

A. V. Kats,[1,*] M. L. Nesterov,[1,2,†] and A. Yu. Nikitin[1,3,‡]

[1]*Theoretical Physics Department, A. Ya. Usikov Institute for Radiophysics and Electronics, Ukrainian Academy of Sciences, 12 Academician Proskura Street, 61085 Kharkov, Ukraine*

[2]*Photonics Research Group, Aston University, Birmingham B4 7ET, United Kingdom*

[3]*Departamento de Física de la Materia Condensada-ICMA, Universidad de Zaragoza, E-50009 Zaragoza, Spain*

(Received 23 February 2007; revised manuscript received 2 June 2007; published 17 July 2007)

We perform a thorough theoretical analysis of resonance effects when an arbitrarily polarized plane monochromatic wave is incident onto a double periodically modulated metal film sandwiched between two transparent media. The proposed theory offers a generalization of the approach that had been developed in our recent papers for the simplest instance of one-dimensional structures to two-dimensional ones. A special emphasis is placed on the films with the modulation caused by cylindrical inclusions; hence, the results obtained are applicable to the films used in the experiments. We discuss a spectral composition of modulated films and highlight the principal role of "resonance" and "coupling" modulation harmonics. All the originating multiple resonances, associated with the surface plasmon-polariton leaky modes, are examined in detail. The transformation coefficients for different diffraction orders are investigated in the vicinity of each resonance. We make a comparison between our theory and recent experiments concerning enhanced light transmittance (ELT) and show the ways of increasing the efficiency of this phenomenon. In the appendixes, we demonstrate a close analogy between the ELT effect and peculiarities of a forced motion of two coupled classical oscillators.

DOI: 10.1103/PhysRevB.76.045413 PACS number(s): 42.25.−p, 73.20.Mf, 78.20.Ci, 78.20.Bh

I. INTRODUCTION

It is exactly significant advances in structuring metals on nanoscales that account for great amount of experimental and theoretical work in the field of plasmonics, which examines resonance optic effects caused by surface plasmon-polariton (SPP) excitation in structured conducting or semiconducting media.[1–3] Over the recent decades, these quasi-two-dimensional (quasi-2D) electrodynamic objects have been thoroughly studied in solid state physics, physics of surfaces, and diffraction optics.[4] SPPs are electromagnetic surface waves coupled to the collective electron excitation. They attract great deal of attention due to their unique possibility of light localization and considerable enhancement of the electric field near the surface.

Great interest in SPPs stems from the latest experiments on enhanced light transmittance (ELT) phenomena. Since 1998, after the observation of Ebbesen and co-workers[5,6] of the violation of Bethe's approach[7] to the diffraction by subwavelength periodic hole arrays in metal films, the ELT has been the subject of numerous studies. Until recently, one of the widely recognized explanations of the ELT through subwavelength periodic hole arrays has been the excitation of SPPs. Most of the authors, who hold on to the SPP conception of ELT, assume that the field enhancement results from "interface" SPPs. The latter can be either single-boundary localized (which is a common case for a nonsymmetric dielectric surrounding of the film) or double-boundary localized for the symmetric surrounding. A periodic hole array acts as a coupler between the incident light and the SPPs. In this context, the crucial point is the surface periodicity. The periodicity caused by other factors, such as corrugation or periodic modulation of the medium electromagnetic properties, etc., also gives rise to the light-matter interaction resonance features, in particular, the ELT effect. Note that making comparison between the ELT transmittance peak positions and those caused by SPP excitation in different diffraction orders undoubtedly points out a significant SPP role (see numerous experiments, e.g., Refs. 5, 6, and 8–14).

It should be noted that the observed ELT effects are strongly dependent on the film surrounding. As the film having the subwavelength hole array is surrounded by the dielectrics with the same dielectric constants (for instance, a freestanding film), the excited SPPs are double-boundary localized, that is, the field is enhanced at both faces of the film (see experiments[8,9]). In this geometry, the ELT in zeroth diffraction order is far more pronounced as compared to the nonsymmetrical film surrounding, when the excited SPPs are single-boundary localized, that is, the field can be increased at a single face of the film. In general, this corresponds to the films deposited onto the quartz substrate. Both of these instances have so far been examined by using numerical methods.[8,9,14–19] Besides, it was shown numerically and experimentally that the ELT occurs for periodic conducting hole-free structures. Basically, this is quite evident since the type of periodicity does not play a crucial role in the excitation of the interface SPPs. In most cases, these were the structures with relief corrugations of the film faces both for symmetrical[20] and nonsymetrical[21–23] dielectric surrounding and the structures with periodically located dielectric pillars.[24]

Several authors have developed an analytical approach which qualitatively describes the ELT. They have examined the diffraction by the film with one-dimensional (1D) periodically modulated dielectric permittivity.[25–30] In these works, a study has been made in the simplest case of a strictly normal incidence onto the symmetrically surrounded film with harmonic modulation of the film permittivity. The

exceptions are Refs. 27 and 30, where the theory is generalized to the nonsymmetric surrounding. The authors of these works have described the zeroth-order transmittance dependence on the parameters for SPP excitation in the first diffraction order. In contrast to their work, we have given a more general analytical insight[31–33] by solving the problem of vector diffraction by the film with nonsymmetric and symmetric dielectric surrounding for arbitrary Fourier spectra of the modulation of the metal permittivity at an arbitrary incident angle and at an arbitrary incident light polarization. The advantage of our analytical treatment is that we not only have described the first-order resonances but have given a classification of the resonances corresponding to single- or double-boundary-localized SPP excitation in single or multiple diffraction orders. Also, we have examined a nonzeroth-order ELT that was observed in the experiments (Refs. 22 and 34). In addition, we refer the reader to Ref. 35, where the alternative analytical approach was suggested to describe the light transmittance through metallic nanoslit structures.

Yet another important class of plasmonic structures possessing interesting diffraction resonance phenomena are metallic nanoparticle arrays.[12,36–38] As known, they can support the so-called *localized-SPP resonances* which are strongly dependent on the shape of individual particles.[38] It is believed that the *shape resonances* similar to the localized ones may affect the ELT in subwavelength hole arrays. The influence of the hole or/and nanoparticle shape was studied experimentally in Refs. 39–41. The study of the conducting films containing periodic lattices of dielectric nanoparticles and voids have been carried out in Refs. 42–44. However, we are not aware of the experimental or theoretical investigation into the optical properties of metallic nanoparticle arrays immersed into a conducting film. Similar to a nanohole array, such a nanoparticle array should display ELT with the wavelength spectra which are strongly dependent on the nanoparticle shape.

In the present paper, we go on examining the resonance optical effects by generalizing the previously developed analytical treatment[31,32] of the conducting films with 2D modulation. We look into the vector diffraction problem for periodically located metallic inclusions in the metal film with an arbitrary dielectric surrounding. Since the inclusions are assumed to be entirely embedded into the film (the faces of the film being flat), the resonances of our system result from the excitation of purely interface SPPs and the localized-SPP resonances do not exist. Apart from the fact that such structures are of interest by themselves, they may be thought of as a model of subwavelength hole arrays, and the approach thus developed is appropriate for other periodical structures (say, for corrugated films). Another essential aspect of our approach is that we can easily describe the polarization of light transmitted or/and reflected by the 2D periodical structure. The polarization properties of subwavelength hole arrays are also a matter of interest, and they have been extensively studied in recent years.[33,45–49]

The paper is arranged as follows. Following the Introduction, in Sec. II, we describe a general approach to the problem of resonance light diffraction by a 2D periodically modulated conducting film for the conical mount and for an arbitrary polarization of the incident light. We stress the fact that the shape of the periodically located inclusions has an impact on the Fourier spectra of the periodical structure and this, in turn, influences the excited SPPs considerably. In Sec. III, we examine the excitation of single-boundary-localized SPPs in the nonsymmetrically sandwiched film, considering both the total transmittance and reflectance spectra and presenting a more detailed analysis of different resonances. We give an explanation of the recently observed polarization dependence on the hole shape[39] from the viewpoint of Fourier spectra of the periodical structure. Besides, we compare our calculations to other recent experiments. Section IV deals with the resonance effects caused by the excitation of double-boundary-localized SPPs in the symmetrically sandwiched film. We make an in-depth study into the fine structure of the two-humped resonance maxima (minima) of the transmittance (reflectance), thereby stressing the role of long-range and short-range SPPs. As far as we know, the fine structure of two-humped resonances for the symmetrically surrounded film has not been examined thoroughly in experiments. In the appendixes below, we draw an analogy between the ELT and the forced oscillations of a well-known classical system of two weakly coupled linear damping mechanical oscillators.

The problem under consideration not only is of profound interest from the purely physical viewpoint but can be widely applied in designing optical subwavelength devices.[4,50] Specifically, SPPs in sandwiched structures have recently come into use as surface plasmon resonance optical sensors,[51–53] and some of them are already commercially available. These sensors are based on the interaction between a waveguide and SPP modes. The basic feature of such real-time high-resolution SPR sensors is that it measures the refractive index variation for biological and chemical domains. It is important to mention that the ELT phenomena are studied in the microwave (terahertz) region of electromagnetic waves,[49,54,55] which attracts great deal of attention.

II. PROBLEM STATEMENT AND MAIN EQUATIONS

A. Analytical approach

Consider an arbitrarily polarized plane monochromatic wave with wave vector $\mathbf{k}$ incident onto a surface of a double periodically modulated metal film surrounded by dielectric media with permittivities ε_τ, $\tau=\pm$, from the medium corresponding to $\tau=-$. We imply that the periodicity is caused by modulation of the dielectric permittivity of a conductor, $\varepsilon=\varepsilon(\mathbf{r}_t)$, $\mathbf{r}_t=(x,y)$, so that $\varepsilon(\mathbf{r}_t)=\varepsilon(\mathbf{r}_t+m_1\boldsymbol{\rho}_1+m_2\boldsymbol{\rho}_2)$, where $\boldsymbol{\rho}_{1,2}$ are elementary translation vectors (see Fig. 1). In what follows, one has to deal with the Fourier expansion of function $\xi(\mathbf{r}_t)=\sqrt{\bar{\varepsilon}}/\varepsilon(\mathbf{r}_t)$, where $\bar{\varepsilon}$ is the mean value of the dielectric permittivity of the metal, $\bar{\varepsilon}=\langle\varepsilon(\mathbf{r})\rangle$. The expansion of this function over $[\bar{\varepsilon}-\varepsilon(\mathbf{r}_t)]/\bar{\varepsilon}$ coincides in the zeroth order with the expansion of the surface impedance, $1/\sqrt{\varepsilon(\mathbf{r}_t)}$, over the same parameter. Therefore, for brevity, name the function $\xi(\mathbf{r}_t)$ surface impedance. Its Fourier representation is written as

$$\xi(\mathbf{r}_t)=\xi_{\mathcal{O}}+\sum_{\mathcal{M}}\tilde{\xi}_{\mathcal{M}}\exp[i(m_1\mathbf{g}_1+m_2\mathbf{g}_2)\cdot\mathbf{r}_t], \qquad (1)$$

where $\tilde{\xi}_{\mathcal{O}}=0$ and $\mathcal{M}$ is the vector index (multi-index), where $\mathcal{M}=(m_1,m_2)$ (integers m_1,m_2 indicate a number of elemen-

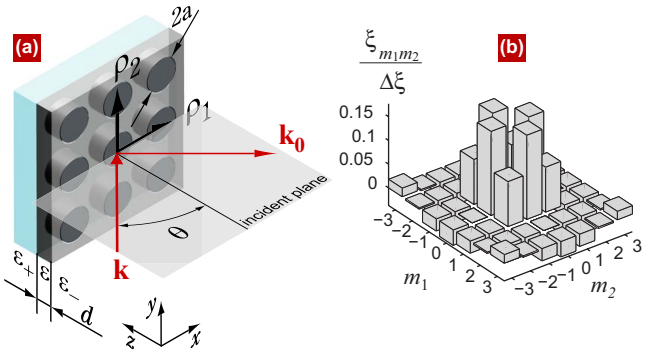

FIG. 1. (Color online) (a) Geometry of the problem. Diffraction by the nonsymmetrically sandwiched 2D modulated metal film (periodical modulation is due to the cylindrical inclusions). (b) Fourier spectrum of a periodical array with $\rho_1=\rho_2=\rho$, $a/\rho=1/3$ shown in (a) [see Eq. (38)].

tary translations along vectors of reciprocal grating, $\mathbf{g}_1,\mathbf{g}_2$); the zero multi-index is $\mathcal{O}\equiv(0,0)$. The electric fields in the dielectric media are written in the form of Rayleigh expansion [the time dependence $\exp(-i\omega t)$ is omitted everywhere]:

$$\mathbf{E}^{\tau}(\mathbf{r}) = \delta_{\tau,-}\mathbf{E}\exp(i\mathbf{k}\cdot\mathbf{r}) + \sum_{\mathcal{M}}\mathbf{E}^{\tau}_{\mathcal{M}}\exp[i\mathbf{k}_{\mathcal{M}t}\cdot\mathbf{r}_t + ik_{\tau|\mathcal{M}z}(z-\delta_{\tau,+}d)], \quad (2)$$

for $z\geqslant d$ ($z\leqslant 0$) if $\tau=+(-)$. Here, d is the film thickness, $\mathbf{E}$ denotes the electric field amplitude of the incident wave, $\mathbf{r}=(x,y,z)$, and the tangential $(\mathbf{k}_t,\mathbf{k}_{\mathcal{M}t})$ and the normal $(k_z,k_{\tau|\mathcal{M}z})$ components of the wave vectors of spatial field harmonics, $\mathbf{k}=\mathbf{k}_t+\mathbf{e}_z k_z$, $\mathbf{k}^{\tau}_{\mathcal{M}}=\mathbf{k}_{\mathcal{M}t}+\mathbf{e}_z k_{\tau|\mathcal{M}z}$, are

$$k_z = k_-\cos\theta, \quad \mathbf{k}_t = k_-(\sin\theta,0,0),$$

$$\mathbf{k}_{\mathcal{M}t} = \mathbf{k}_t + m_1\mathbf{g}_1 + m_2\mathbf{g}_2,$$

$$k_{\tau|\mathcal{M}z} = \tau\sqrt{k_\tau^2-\mathbf{k}^2_{\mathcal{M}t}}, \quad k_\tau=\sqrt{\varepsilon_\tau}k, \quad k=\omega/c, \quad (3)$$

where θ is the angle of incidence, $\mathrm{Re}(\tau k_{\tau|\mathcal{M}z})$, $\mathrm{Im}(\tau k_{\tau|\mathcal{M}z})\geqslant 0$. Similar to Refs. 31–33, we will take into account the modulation in the boundary conditions only, so that within the conducting film we seek the solution in the form

$$\bar{\mathbf{E}}(\mathbf{r}) = \sum_{\mathcal{M},\tau}\bar{\mathbf{E}}^{\tau}_{\mathcal{M}}\exp(\tau\tilde{k}z + i\mathbf{k}_{\mathcal{M}t}\cdot\mathbf{r}_t),$$

$$\tilde{k} = k\sqrt{-\bar{\varepsilon}}, \quad 0\leqslant z\leqslant d. \quad (4)$$

We introduce polarization unit vectors,

$$\mathbf{e}^{\tau|+}_{\mathcal{M}} = \frac{\mathbf{e}_z\times\mathbf{k}_{\mathcal{M}t}}{k_{\mathcal{M}t}}, \quad \mathbf{e}^{\tau|-}_{\mathcal{M}} = \frac{\mathbf{e}^{\tau|+}_{\mathcal{M}}\times\mathbf{k}^{\tau}_{\mathcal{M}}}{k_\tau},$$

$$\mathbf{e}^{-|+} = \frac{\mathbf{e}_z\times\mathbf{k}_t}{k_t}, \quad \mathbf{e}^{-|-} = \frac{\mathbf{e}^{-|+}\times\mathbf{k}}{k_-}, \quad (5)$$

where $\mathbf{e}^{\tau|\sigma}_{\mathcal{M}}$ are for TM (TE) or p (s) polarization for $\sigma=-(+)$ in the $\mathcal{M}$th diffraction order in the dielectric media τ, and $\mathbf{e}^{-|\sigma}$ are polarization basis vectors for the incident wave. In terms of the polarization vectors, the electric and magnetic fields in the dielectric media are

$$\begin{bmatrix}\mathbf{E}^{\tau}_{\mathcal{M}}\\ \mathbf{H}^{\tau}_{\mathcal{M}}\end{bmatrix} = \sum_{\sigma}\begin{bmatrix}E^{\tau|\sigma}_{\mathcal{M}}\\ H^{\tau|\bar{\sigma}}_{\mathcal{M}}\end{bmatrix}\mathbf{e}^{\tau|\sigma}_{\mathcal{M}}, \quad \begin{bmatrix}\mathbf{E}\\ \mathbf{H}\end{bmatrix} = \sum_{\sigma}\begin{bmatrix}E^{\sigma}\\ H^{\bar{\sigma}}\end{bmatrix}\mathbf{e}^{-|\sigma}, \quad (6)$$

where $\bar{\sigma}\equiv-\sigma$. As we neglect the permittivity modulation inside the film, the internal fields are divergence-free. Thus, they can be decomposed into a form similar to Eq. (6).

Introducing the transformation coefficients (TCs) $T^{\tau|\sigma\sigma'}_{\mathcal{M}}$,

$$E^{\tau|\sigma}_{\mathcal{M}} = \sum_{\sigma'}T^{\tau|\sigma\sigma'}_{\mathcal{M}}E^{\sigma'}, \quad (7)$$

and excluding the internal fields from the boundary conditions, we arrive at the following infinite linear system for the TCs of the outer fields:

$$\sum_{\mathcal{M}',\tau',\sigma''}D^{\tau\tau'|\sigma\sigma''}_{\mathcal{M}\mathcal{M}'}T^{\tau'|\sigma''\sigma'}_{\mathcal{M}'} = V^{\tau|\sigma\sigma'}_{\mathcal{M}}. \quad (8)$$

The matrix $D^{\tau\tau'|\sigma\sigma''}_{\mathcal{M}\mathcal{M}'}$ and the right-hand side vectors $V^{\tau|\sigma\sigma'}_{\mathcal{M}}$ are linear relative to the modulation,

$$D^{\tau\tau'|\sigma\sigma'}_{\mathcal{M}\mathcal{M}'} = \delta_{\mathcal{M}\mathcal{M}'}\delta_{\sigma\sigma'}b^{\tau\tau'|\sigma}_{\mathcal{M}} + d^{\tau\tau'|\sigma\sigma'}_{\mathcal{M}\mathcal{M}'},$$

$$V^{\tau|\sigma\sigma'}_{\mathcal{M}} = \delta_{\mathcal{M},\mathcal{O}}\delta_{\sigma\sigma'}V^{\tau|\sigma}_{\mathcal{O}} + v^{\tau|\sigma\sigma'}_{\mathcal{M}}. \quad (9)$$

The modulation-independent terms are diagonal both with respect to the diffraction order and polarization. Explicitly,

$$b^{\tau\tau'|\sigma}_{\mathcal{M}} = \tau'\sigma[\delta_{\tau\tau'}\varepsilon_{\tau'}^{-(1+\sigma)/4}\beta^{(1-\sigma)/2}_{\tau'|\mathcal{M}}\tanh\Phi + (\bar{\sigma})^{(1-\tau')/2}\tau^{(\sigma+1)/2}\xi_{\mathcal{O}}(\beta_{\tau'|\mathcal{M}}\sqrt{\varepsilon_{\tau'}})^{(1+\sigma)/2}]\times(\cosh\Phi)^{(1+\tau\tau')/2},$$

$$V^{\tau|\sigma}_{\mathcal{O}} = [\delta_{\tau,-}\varepsilon_-^{-(1+\sigma)/4}\beta^{(1-\sigma)/2}_{-|\mathcal{O}}\tanh\Phi + \sigma\tau^{(\sigma+1)/2}\xi_{\mathcal{O}}(\beta_{-|\mathcal{O}}\sqrt{\varepsilon_-})^{(1+\sigma)/2}](\cosh\Phi)^{(1-\tau)/2}. \quad (10)$$

Here,

$$\Phi \equiv \tilde{k}d, \quad (11)$$

the real part of Φ is the film thickness in the skin depths, and $\beta_{\tau|\mathcal{M}}$ is the normalized z component of the $\mathcal{M}$th spatial field harmonic wave vector, which is related to the tangential component $\boldsymbol{\alpha}_{\mathcal{M}}$ as

$$\beta_{\tau|\mathcal{M}} = \frac{\tau k_{\tau|\mathcal{M}z}}{k\varepsilon_\tau} = \frac{\sqrt{\varepsilon_\tau-\alpha^2_{\mathcal{M}}}}{\varepsilon_\tau}, \quad \boldsymbol{\alpha}_{\mathcal{M}} = \mathbf{k}_{\mathcal{M}t}/k. \quad (12)$$

The nondiagonal terms are

$$d^{\tau\tau'|\sigma\sigma'}_{\mathcal{M}\mathcal{M}'} = \tau^{(\sigma+1)/2}\sigma^{(1-\sigma')/2}(\sigma')^{(1-\tau')/2}S^{\sigma\cdot\sigma'}_{\mathcal{M}\mathcal{M}'}\tilde{\xi}_{\mathcal{M}-\mathcal{M}'}\times(\beta_{\tau'|\mathcal{M}'}\sqrt{\varepsilon_{\tau'}})^{(1+\sigma')/2}(\cosh\Phi)^{(1+\tau\tau')/2},$$

$$v_{\mathcal{M}}^{\tau|\sigma\sigma'} = \sigma' d_{\mathcal{MO}}^{\tau-|\sigma\sigma'}. \tag{13}$$

$S^{+}_{\mathcal{MM}'}$ ($S^{-}_{\mathcal{MM}'}$) are sines (cosines) of the angle $\psi_{\mathcal{MM}'} = (\boldsymbol{\alpha}_{\mathcal{M}}, \hat{\boldsymbol{\alpha}}_{\mathcal{M}'})$ between vectors $\boldsymbol{\alpha}_{\mathcal{M}}$ and $\boldsymbol{\alpha}_{\mathcal{M}'}$,

$$S^{\sigma}_{\mathcal{MM}'} \equiv \begin{cases} \dfrac{\boldsymbol{\alpha}_{\mathcal{M}} \cdot \boldsymbol{\alpha}_{\mathcal{M}'}}{\alpha_{\mathcal{M}} \alpha_{\mathcal{M}'}} = \cos\psi_{\mathcal{MM}'}, & \sigma = + \\ \dfrac{\mathbf{e}_z \cdot (\boldsymbol{\alpha}_{\mathcal{M}} \times \boldsymbol{\alpha}_{\mathcal{M}'})}{\alpha_{\mathcal{M}} \alpha_{\mathcal{M}'}} = \sin\psi_{\mathcal{MM}'}, & \sigma = - . \end{cases} \tag{14}$$

The resonances in the system are due to the existence of the eigenmodes in the film, i.e., SPPs. When an evanescent field harmonic is close to the grazing one, its amplitude increases substantially as the process of eigenmode excitation occurs. For infinitesimal modulation, the eigenmodes of the film are initial SPPs, with the dispersion relation corresponding to the determinant of the matrix $\|D^{\tau\tau'|\sigma\sigma''}_{\mathcal{MM}'}\|$ vanishing in zeroth-order approximation in modulation. Then, $\det\|D^{\tau\tau'|\sigma\sigma''}_{\mathcal{MM}'}\|$ becomes an infinite product of $\|b^{\tau\tau'|\sigma}_{\mathcal{M}}\|$ determinants, so that each of them corresponds to a certain SPP eigenmode of the unmodulated film. The equation $\det\|b^{\tau\tau'|\sigma}_{\mathcal{M}}\| = 0$ has the physical roots for $\sigma = -$ only, which conforms to p polarization:

$$(\beta_{+|\mathcal{M}} \tanh\Phi + \xi_{\mathcal{O}})(\beta_{-|\mathcal{M}} \tanh\Phi + \xi_{\mathcal{O}})\cosh^2\Phi - \xi^2_{\mathcal{O}} = 0. \tag{15}$$

For a rather thick film, $\exp(\Phi') \gg 1$ [here and below, the prime ($'$) and the double prime ($''$) indicate the real and the imaginary parts of the physical value], SPPs in the film are close to those existing at the boundary between the metal and each of the dielectric half-spaces, and are single-boundary-localized (SB) SPPs. These modes are governed by the dispersion relation

$$\beta_{\tau|\mathcal{M}} + \xi_{\mathcal{O}} = 0, \tag{16}$$

where $\tau = +(-)$ is for the metal-substrate (superstrate) SB SPP. The symmetric surrounding (for instance, a freestanding film) is a particular instance because the solutions of Eq. (16) for different τ coincide.[56] Then, the initial SPPs existing at the boundary of the metal and dielectric half-space become coupled due to the finite film thickness, and one obtains the two double-boundary-localized (DB) SPP modes: long-range (LR) and short-range (SR) SPPs.[57,58] For $\varepsilon_+ = \varepsilon_- \equiv \varepsilon$, and, respectively, $\beta_{+|\mathcal{M}} = \beta_{-|\mathcal{M}} \equiv \beta_{\mathcal{M}}$, one finds from Eq. (15) the two roots, $\beta_{\mathcal{M}} = \beta^{\pm}_{\mathcal{M}}$,

$$\beta^{l}_{\mathcal{M}} = -\xi_{\mathcal{O}} \tanh(\Phi/2), \quad \beta^{s}_{\mathcal{M}} = -\xi_{\mathcal{O}} \coth(\Phi/2), \tag{17}$$

that is, the single-boundary-localized modes coupled into double-boundary-localized ones. Therefore, the frequencies of initial SPPs are split, the spectral degeneration vanishes, and we arrive at two different eigenfrequencies described by Eq. (17). Here, superscript l (s) stays for the LR (SR) SPP. The LR (SR) mode possesses a high- (low-) frequency and is related to the antisymmetric (symmetric) surface charge distribution with respect to the midplane $z = d/2$ and the spatial distribution of the electric field component tangential to the film faces. As a result, the SR SPP is characterized by higher Ohmic losses.

Since the modulation is assumed to be small, the eigenmodes of the modulated film ("dressed" modes) differ slightly from those existing in the unmodulated film. If the dressed SPP eigenmodes include the propagating field harmonics, they become leaky modes and thus can be coupled with ingoing waves. The dispersion relation of the dressed SPP modes defines the resonance conditions. However, to identify the resonance type, the modulation can be neglected. Bearing in mind that $\beta_{\mathcal{M}|\tau}$ depends on the incidence angle θ and the wavelength λ, it is possible to consider the imaginary part of Eq. (16) as the "resonance curve" in a θ-λ plane. In fact, the left-hand side of Eq. (16) is nothing else than the denominator of the SPP propagator (Green's function of the boundary of the metal half-space). Therefore, the imaginary part of Eq. (16) yields the closest-to-the-pole point on the imaginary axis in a complex β plane. This point is related to strong peculiarities in TCs when the pole is close to the imaginary axis (that is, when $\xi' \ll |\xi''|$, which holds for noble metals starting from the visible region of the spectrum). For instance, in the case of rectangular symmetry, $\mathbf{g}_1 \perp \mathbf{g}_2$, $g_1 = g_2$, the imaginary part of Eq. (16) reads

$$(\sin\theta\cos\psi + m_1\kappa_1)^2 + (\sin\theta\sin\psi + m_2\kappa_2)^2 = K^2_{\tau}, \tag{18}$$

where ψ is the angle of the incident plane orientation relative to $\mathbf{g}_1$ (say, "tilting" angle), $\kappa_{1,2} = g_{1,2}/k = \lambda/\rho_{1,2}$, and $K_{\tau} = \sqrt{\varepsilon_{\tau} + \varepsilon^2_{\tau}\xi''^2_{\mathcal{O}}}$ is the SPP dimensionless wave vector. We designate the curve given by Eq. (18) as $(m_1, m_2)_{\tau}$. All points of the θ-λ plane may be classified as follows.[59] If a point does not belong to any resonance curve, we have a nonresonance diffraction case. If a point belongs to a single curve with a fixed $\mathcal{M}$ and τ, we obtain a *single diffraction-order single-boundary resonance*. If a point serves as the intersection of several curves having different multi-indexes $\{\mathcal{M}, \mathcal{M}', \mathcal{M}'', \ldots\}$, but the same τ value, then we obtain a *multiple diffraction-order single-boundary resonance*. Note that for specific geometry of high symmetry, $\psi = 0$ and $\psi = \pi/2$, the curves for different signs of m_2 and m_1 coincide; when $\psi = \pi/4$, curves $(m_1, m_2)_{\tau}$ and $(m_2, m_1)_{\tau}$ are indistinguishable as well. The intersection of two resonance curves with different τ yields the point of a *double-boundary resonance*. When DB SPPs have a unique multi-index $\mathcal{M}$, we then arrive at a *single diffraction-order double-boundary resonance* (SDB). SDB resonance only occurs for the symmetric surrounding of the film, $\varepsilon_+ = \varepsilon_-$. Here, the initial surface modes are coupled mainly through the finite film thickness and, by and large, the corresponding dependences of the reflectance and/or transmittance are of two-valley (two-peak) shape due to splitting of LR and SR modes. The explicit form of the resonance curve corresponding to LR (SR) SPP resonances coincides with that given by Eq. (18), if $\xi''_{\mathcal{O}}$ is replaced by $\xi''_{\mathcal{O}} \tanh(\Phi'/2)$ [$\xi''_{\mathcal{O}} \coth(\Phi'/2)$] in the designation of K_{τ} in Eq. (18). When DB SPPs are related to different multi-indexes (*multiple diffraction-order double-boundary resonance*), which occurs under very specific conditions,

they are simultaneously coupled through periodicity and the finite film thickness.

Now, take up the solution of the system (8). In a small region of the θ-λ plane, which is of order of the resonance width, the solution is strongly dependent on the number of resonance curves passing through this region. Hence, it is convenient to subdivide the set of the diffraction orders into a resonance subset, $\mathfrak{R}$, which contains the multi-indexes relative to the above-mentioned curves, and a nonresonance subset, $\mathfrak{N}$. Thus, we subdivide the initial infinite system into the resonance subsystem with the resonance TCs and the nonresonance subsystem having the nonresonance TCs. The resonance TCs are related to p components of the TCs defined by the resonance multi-indexes, and the nonresonance TCs correspond to s components of amplitudes with the resonance multi-indexes, $T_{\mathcal{R}}^{\tau|+\sigma}$, and both p and s components of TCs with nonresonance multi-indexes, $T_{\mathcal{N}}^{\tau|\sigma\sigma'}$, $\mathcal{N}\in\mathfrak{N}$.

In the main approximation,[31–33] which assumes retaining the quadratic-in-modulation amplitude terms in the matrix elements, and the linear terms in the right-hand sides, the resonance subsystem becomes

$$\sum_{\tau',\mathcal{R}'} B_{\mathcal{R}\mathcal{R}'}^{\tau\tau'} T_{\mathcal{R}'}^{\tau'|-\sigma} = \tilde{V}_{\mathcal{R}}^{\tau|\sigma}, \tag{19}$$

where

$$B_{\mathcal{R}\mathcal{R}'}^{\tau\tau'} = \delta_{\mathcal{R}\mathcal{R}'} b_{\mathcal{R}}^{\tau\tau'|-} + d_{\mathcal{R}\mathcal{R}'}^{\tau\tau'|-} - \overline{\sum_{\mathcal{M},\sigma''}} \sum_{\tau'',\tau'''} d_{\mathcal{R}\mathcal{M}}^{\tau\tau''|-\sigma''} (\hat{b}^{-1})_{\mathcal{M}}^{\tau''\tau'''|\sigma''} d_{\mathcal{M}\mathcal{R}'}^{\tau'''\tau'|\sigma''-}, \tag{20}$$

$$\tilde{V}_{\mathcal{R}}^{\tau|\sigma} = V_{\mathcal{R}}^{\tau|\sigma} - \bar{\delta}_{\mathfrak{R}\mathcal{O}}^{(1-\sigma)/2} \sum_{\tau',\tau''} d_{\mathcal{R}\mathcal{O}}^{\tau\tau'|-\sigma} (\hat{b}^{-1})_{\mathcal{O}}^{\tau'\tau''|\sigma} V_{\mathcal{O}}^{\tau''|\sigma}. \tag{21}$$

Here, $\hat{b} \equiv \|b_{\mathcal{M}}^{\tau\tau'|\sigma}\|$, and the sum with the overline ($\bar{\Sigma}$) means that the terms with the superscript $\sigma''=-$ and a resonance diffraction order $\mathcal{M}=\mathcal{R}\in\mathfrak{R}$ have to be omitted. The function $\bar{\delta}_{\mathfrak{R}\mathcal{O}}$ is equal to 0 if within the resonance indexes there is the zeroth one, and to 1 otherwise. The zero value of matrix $\hat{B}$ determinant yields a dispersion relation of the SPP modes in the film in the main approximation. As was discussed above, the block, $b_{\mathcal{R}}^{\tau\tau'|-}$, being diagonal relative to the diffraction order, contributes to the unperturbed dispersion relation. The nondiagonal, linear-in-modulation block, $d_{\mathcal{R}\mathcal{R}'}^{\tau\tau'|--}$, contains the "inter-resonance" or "coupling" modulation harmonic, $\tilde{\xi}_{\mathcal{R}-\mathcal{R}'}$, which is chiefly responsible for the SPP dispersion curve splitting and for the appearance of the spectral band gap.[60,61] The third term in Eq. (20) is quadratic in modulation and describes the second-order scattering processes which results in the broadening and the shift of the dispersion branches.

The nonresonance TCs, $T_{\mathcal{N}}^{\tau|\sigma\sigma'}$, are expressed in terms of the resonance TCs as

$$T_{\mathcal{N}}^{\tau|\sigma\sigma'} \simeq \delta_{\mathcal{N},\mathcal{O}}\delta_{\sigma\sigma'} T_F^{\tau|\sigma} - \sum_{\tau',\tau''} (\hat{b}^{-1})_{\mathcal{N}}^{\tau\tau'|\sigma} d_{\mathcal{N}\mathcal{R}}^{\tau'\tau''|\sigma-} T_{\mathcal{R}}^{\tau''|-\sigma'}, \tag{22}$$

where $T_F^{\tau|\sigma}$ is a transmission (for $\tau=+$) or a reflection (for $\tau=-$) coefficient associated with p (at $\sigma=-$) or s (at $\sigma=+$) polarization for an unmodulated film. s components of the TCs with the resonance multi-indexes, $T_{\mathcal{R}}^{\tau|+\sigma}$, are expressed in terms of p components, $T_{\mathcal{R}}^{\tau|-\sigma}$, and are small as compared with the latter; they are of no interest, and we do not present them herein. The diffraction efficiencies are

$$\tau_{\mathcal{M}} = \frac{|\mathbf{E}_{\mathcal{M}}^{+}|^2}{|\mathbf{E}|^2} \cdot \frac{\mathfrak{R}e(k_{+|\mathcal{M}z})}{k_z}, \quad \rho_{\mathcal{M}} = \frac{|\mathbf{E}_{\mathcal{M}}^{-}|^2}{|\mathbf{E}|^2} \cdot \frac{\mathfrak{R}e(k_{-|\mathcal{M}z})}{k_z}.$$

From the energy conservation, it evidently follows that

$$1 - \sum_{\mathcal{M}} [\rho_{\mathcal{M}} + \tau_{\mathcal{M}}] = \mathcal{P} \geqslant 0, \tag{23}$$

where $\mathcal{P} \sim \int \varepsilon'' |\bar{\mathbf{E}}|^2 dz$ is the absorbed part of the energy flux density.

B. Single diffraction-order resonance

If a certain point of the λ-θ plane belongs to one or two curves [Eq. (18)] having a single multi-index $\mathcal{R}=(r_1,r_2)$ (for other parameters being fixed), the vicinity of this point defines a single diffraction-order resonance. Moreover, according to the above classification, a SB resonance is associated with a curve characterized by a single τ, while the intersection of two curves with different τ values yields a DB resonance. The resonance TCs are then similar to those obtained for 1D modulation (see Ref. 33),

$$\begin{bmatrix} T_{\mathcal{R}}^{\tau|-+} \\ T_{\mathcal{R}}^{\tau|--} \end{bmatrix} = \begin{bmatrix} -\cos\theta \sin\psi_{\mathcal{R}\mathcal{O}} \\ \cos\psi_{\mathcal{R}\mathcal{O}} \end{bmatrix} L_{\mathcal{R}}^{\tau} \tilde{\xi}_{\mathcal{R}} [\exp(-\Phi)]^{(1+\tau)/2}, \tag{24}$$

where

$$L_{\mathcal{R}}^{\tau} = 2\pi(\tilde{\beta}_{\bar{\tau}|\mathcal{R}} - \delta_{\tau,+}\Upsilon_{\mathcal{R}})\Delta_{\mathcal{R}}, \tag{25}$$

$$\tilde{\beta}_{\tau|\mathcal{R}} = \beta_{\tau|\mathcal{R}} \tanh\Phi + \xi_{\mathcal{O}} + G_{\mathcal{R}}^{\tau}, \tag{26}$$

$$\Delta_{\mathcal{R}} = \tilde{\beta}_{+|\mathcal{R}}\tilde{\beta}_{-|\mathcal{R}} - \Upsilon_{\mathcal{R}}^2 \cosh^{-2}\Phi, \quad \Upsilon_{\mathcal{R}} = \xi_{\mathcal{O}} + G_{\mathcal{R}}^{+} + G_{\mathcal{R}}^{-}, \tag{27}$$

$$G_{\mathcal{R}}^{\tau} = -\sum_{\mathcal{N}} \frac{\tilde{\xi}_{\mathcal{R}-\mathcal{N}}\tilde{\xi}_{\mathcal{N}-\mathcal{R}}}{\beta_{\tau|\mathcal{N}}} (\cos^2\psi_{\mathcal{R}\mathcal{N}} + \varepsilon_{\tau}\beta_{\tau|\mathcal{N}}^2 \sin^2\psi_{\mathcal{R}\mathcal{N}}). \tag{28}$$

Note that $T_{\mathcal{R}}^{\tau|+\sigma} \sim O(\tilde{\xi}_{\mathcal{R}})$, $|T_{\mathcal{R}}^{\tau|-\sigma}| \gg |T_{\mathcal{R}}^{\tau|+\sigma}|$. The resonance TCs have two poles. For a nonsymmetric surrounding, these poles are related to SPPs existing at the opposite film faces, while in a symmetric surrounding, they are related to LR and SR SPP modes.

The structure of the resonance TCs reveals that the coupling strength between the incident wave and the SPP excited is proportional to the scalar product of the SPP and the incident-wave magnetic fields. Note that the SPP magnetic field is orthogonal to its propagation direction and is parallel to the interface. Therefore, the SPP is dramatically excited by the projection of the tangential component of the incident-wave magnetic field onto $\mathbf{H}^{\tau}_{\mathcal{R}t}$ (or, alternatively, by the scalar product of tangential components of the electric SPP fields and the incident wave). As to p (s) polarization of the incident light, the projection is $H_t \cos\psi_{\mathcal{R}\mathcal{O}}$ ($H_t \cos\theta \sin\psi_{\mathcal{R}\mathcal{O}}$), where $\psi_{\mathcal{R}\mathcal{O}}$ is the angle between $\mathbf{H}^{\tau}_{\mathcal{R}t}$ and $\mathbf{H}_t$. For instance, with the incidence of purely p- (s-) polarized light, the SPPs propagating parallel (perpendicular) to the incidence plane cannot be excited, even if wave vector $\mathbf{k}_{\mathcal{R}t}$ is close to the poles in Eq. (24).

The zeroth-order polarization matrix is

$$\begin{pmatrix} T^{\tau|++}_{\mathcal{O}} & T^{\tau|+-}_{\mathcal{O}} \\ T^{\tau|-+}_{\mathcal{O}} & T^{\tau|--}_{\mathcal{O}} \end{pmatrix} = \begin{pmatrix} T^{\tau|+}_{F} & 0 \\ 0 & T^{\tau|-}_{F} \end{pmatrix} + \begin{pmatrix} 2\cos\theta_\tau \cos\theta \sin^2\psi_{\mathcal{R}\mathcal{O}} & -\cos\theta_\tau \sin 2\psi_{\mathcal{R}\mathcal{O}} \\ -\tau\cos\theta\sin 2\psi_{\mathcal{R}\mathcal{O}} & 2\tau\cos^2\psi_{\mathcal{R}\mathcal{O}} \end{pmatrix} L^{\tau}_{\mathcal{O}|\mathcal{R}}, \tag{29}$$

where

$$L^{\tau}_{\mathcal{O}|\mathcal{R}} = -\frac{\sqrt{\varepsilon_\tau}\tilde{\xi}_{\mathcal{R}}\tilde{\xi}_{-\mathcal{R}}}{\cos\theta_\tau \Delta_{\mathcal{R}}}[\tilde{\beta}_{\tau|\mathcal{R}} + (\tilde{\beta}_{\tau|\mathcal{R}} - \Upsilon_{\mathcal{R}})(\cosh\Phi)^{\tau-1}] \times (\cosh\Phi)^{-(1+\tau)/2}. \tag{30}$$

θ_τ is the angle of propagation of the zeroth-order wave in the τth dielectric media relative to the Oz axis (in the superstrate $\theta_- \equiv \theta$). The structure of these coefficients shows an interference caused by the competition between the nonresonance channel (the terms $T^{\tau|\sigma}_F$) and the resonance channel [the second terms in Eq. (29), which are proportional to $\tilde{\xi}_{\mathcal{R}}\tilde{\xi}_{-\mathcal{R}}/\Delta_{\mathcal{R}}$]. The nonresonance term should be retained for the zeroth-order reflectance, since it is of order of unity, $|T^{\tau|\sigma}_F| \sim 1$. Otherwise, for a rather strong resonance it can be neglected for the transmittance in the vicinity of the resonance maxima, since $|T^{+|\sigma}_F| \sim |\xi_{\mathcal{O}}|\exp(-\Phi') \ll 1$ and is much smaller than the resonance input into the transmittance.

The wavelength resonance width, $\Delta\lambda/\lambda$, is contributed both from the dissipation losses, being proportional to $\xi'_{\mathcal{O}}$, and from the radiation losses due to SPP scattering into the outgoing propagating waves. It is of order $\Delta\lambda/\lambda \sim |\xi''_{\mathcal{O}}|[\xi'_{\mathcal{O}} + O(|\tilde{\xi}^2|)]$, as it follows from Eqs. (24)–(30). The term proportional to $O(|\tilde{\xi}^2|)$ results from the radiation losses and in the simplest case may be represented approximately as $\Sigma_{\mathcal{N}} C_{\mathcal{N}} \tilde{\xi}_{\mathcal{R}-\mathcal{N}} \tilde{\xi}_{\mathcal{N}-\mathcal{R}}/\beta_{\tau|\mathcal{N}}$, where $|C_{\mathcal{N}}| \sim 1$, and the summation is done over those $\mathcal{N}$ that satisfy $\mathrm{Im}(\beta_{\tau|\mathcal{N}})=0$. According to the formulas describing the resonance and zeroth-order TCs, the *optimal amplitude* of the resonance harmonic is $|\tilde{\xi}_{\mathcal{R}}| \sim \sqrt{\xi'_{\mathcal{O}}}$ and this gives rise to the resonance width of order $\Delta\lambda/\lambda \sim \xi'_{\mathcal{O}}|\xi''_{\mathcal{O}}|$. The optimal amplitude is related to the maximal SPP excitation and, consequently, to the minimal (maximal) reflectance (transmittance) value. Although we assume the modulation to be rather small, let us make a rough estimate of the resonance width for the hole arrays. For Ag films in the visible and near infrared frequency region, the impedance of the film is $|\xi_f| \sim 10^{-1}$, while for the holes the impedance is $|\xi_i| \sim 1$. Therefore, $|\tilde{\xi}_{\mathcal{R}}| \sim |\Delta\xi| \sim 1 \gg \xi'_{\mathcal{O}}$ and $\Delta\lambda/\lambda \sim |\xi''_{\mathcal{O}}| \sim 10^{-1}$. For wavelength of order $\lambda \sim 1$ μm, the resonance width can be estimated as $\Delta\lambda \sim 100$ nm, which is in good qualitative agreement with numerous experimental results (see, e.g., Refs. 5, 6, and 8). In the experiments, the resonance width is equally affected by the nonplane character of an input light wave and the finiteness of the periodic array.

Note that the resonance width is very important for subdiffraction-limited optical imaging (optics of volume or surface "superlenses"). Sufficiently broadened SPP resonances may be efficiently used to enhance the evanescent modes and thus to gain the subwavelength information on nanoobjects (see Ref. 62).

C. Multiple resonances

The approach that we have developed allows considering the diffraction problem for the resonances of arbitrary multiplicity on 2D periodical structures with an arbitrary symmetry. However, from the experimental point of view the resonances of fourfold multiplicity, which occur in the normal incidence, $\theta=0$, on the square and rectangular periodical arrays are of special interest. Here, and in what follows, we will concentrate on the structures with C_{2v} symmetry: $\tilde{\xi}(\hat{C}_{2v}\mathbf{r}_t) = \tilde{\xi}(\mathbf{r}_t)$; the geometrical symmetry (Brillouin zone symmetry) is assumed to be C_{4v}, i.e., $\mathbf{g}_1$ is perpendicular to $\mathbf{g}_2$ and their modules are equal, $g_1 = g_2$. As evident from Eq. (18), at normal incidence the multiple SPP resonances arise at wavelengths of $\lambda^{\tau}_{r_1,r_2} = \rho K_\tau/\sqrt{r_1^2+r_2^2}$, where ρ is the period of the structure. Points $\theta=0$, $\lambda=\lambda^{\tau}_{r_1,r_2}$ in the θ-λ plane are the intersections of four resonance curves for the single τ (SB resonance) or eight curves for both $\tau=\pm$ (DB resonance in symmetric surrounding). We label a fourfold SB resonance as $[r_1,r_2]_\tau$, which is consistent with the intersection of the following resonance curves: $(r_1,r_2)_\tau$, $(-r_1,r_2)_\tau$, $(r_1,-r_2)_\tau$, and $(-r_1,-r_2)_\tau$. A fourfold DB resonance is denoed as $[r_1,r_2]$. In addition, if all the values of a certain function $F_{\mathcal{M}}$ with subscripts from the above subsets are equal, we designate it by $F_{[r_1,r_2]}$.

Similar to the single resonance, the pair of field harmonics with wave vectors $\mathbf{k}_{(r_1,r_2)t} = r_1\mathbf{g}_1 + r_2\mathbf{g}_2$ and $\mathbf{k}_{(-r_1,-r_2)t} = -r_1\mathbf{g}_1$

$-r_2\mathbf{g}_2$ for the fourfold resonance is efficiently generated by the projection of the incident-wave magnetic field onto the direction perpendicular to $\mathbf{k}_{(r_1,r_2)t}$ (the direction of the SPP magnetic field with this wave vector), viz., by $H\sin\phi_{r_1,r_2}$, where $\phi_{\mathcal{R}}$ is the angle between $\mathbf{k}_{\mathcal{R}t}$ and $\mathbf{H}_t=\mathbf{H}$. By analogy, the amplitudes of the field harmonics with diffraction indexes $(\pm r_1, \mp r_2)$ are proportional to $H\sin\phi_{-r_1,r_2}$. Thus, for special polarization of the incident wave, at $\phi_{\mathcal{R}}=0,\pm\pi,\pm\mathcal{R}$ the resonance field harmonics are not excited via the first-order scattering process (but rather via the higher-order processes). This leads to twofold reduction in multiplicity of the resonance in the main approximation. For an arbitrary polarized incident wave, the polarizations of the zeroth-order transmitted and reflected waves are formed mainly due to single backscattering by the interference contribution of all resonance field harmonics. Also, they are contributed from the zeroth-order components related to the "scatteringless" reflection and transmission for an unmodulated film. Otherwise, the polarizations of both propagating and evanescent nonresonance field harmonics are formed chiefly by single scattering from the zeroth diffraction order and from all the resonance diffraction orders.

For the structures with C_{2v} modulation symmetry, the solution of Eq. (19) is substantially simplified in the vicinity of normal incidence. For $[r,0]$ or $[r,0]_\tau$ resonance, the resonance TCs are similar to those given in Eq. (24) [see the explicit expressions in Appendix B, Eq. (B1)]. Nevertheless, in $\tilde{\beta}_{\tau|\mathcal{R}}$ a linear-in-modulation term $(\tilde{\xi}_{2\mathcal{R}})$ arises, which is the inter-resonance harmonic responsible for the splitting and shifting of the resonance.

To get a better understanding of the resonance diffraction, consider the eigenmodes of C_{2v} structures. They are defined approximately by the relation $\hat{B}\hat{T}=0$. In particular, the eigenfrequencies may be found from the equation $\det\hat{B}=0$. For a rather thick film, $\exp(-\Phi')\ll 1$, the eigenmode structure of SB SPPs can be obtained in the approximation of the half-space problem (see the detailed analytical treatment in Ref. 60). Thus, we restrict ourselves to the eigenmodes that are close to those existing at the metal-dielectric interface and not coupled through a film thickness. Bearing in mind the homogeneous problem statement, we must make some change in the notations so that one of the resonance $\mathbf{k}$ vectors in the diffraction problem, $\mathbf{k}_{\mathcal{R}t}$, becomes the SPP quasi-wave-vector $\mathbf{q}$ ending in some Brillouin zone. The other wave vectors close to the resonance conditions are for the "resonance satellites" that constitute a coupled SPP state.

Concentrate first on the simplest example of a twofold coupling through the periodicity. Suppose that the resonance wave vectors are $\mathbf{k}_{Rt}\to\mathbf{q}$ and $\mathbf{k}_{R't}\to\mathbf{q}'$. Then, we can consider the diagonal in τ homogeneous subsystems of the resonance system (19) which has two TCs, for the diffraction orders $\mathcal{R}=(r_1,r_2)$ and $\mathcal{R}'=(r_1',r_2')$. Using Eqs. (10)–(14) (and assuming $\tanh\Phi=1$), we present it as

$$\begin{pmatrix} \beta_{\tau|\mathcal{R}}+\xi_{\mathcal{O}} & \tilde{\xi}_{\Delta\mathcal{R}}\cos\psi_{\mathcal{R}\mathcal{R}'} \\ \tilde{\xi}_{-\Delta\mathcal{R}}\cos\psi_{\mathcal{R}\mathcal{R}'} & \beta_{\tau|\mathcal{R}'}+\xi_{\mathcal{O}} \end{pmatrix}\begin{pmatrix} E^{\tau}_{\mathcal{R}z} \\ E^{\tau}_{\mathcal{R}'z} \end{pmatrix}=0. \quad (31)$$

Here, $\Delta\mathcal{R}=\mathcal{R}-\mathcal{R}'$, and we omit the quadratic-in-modulation amplitude terms, supposing that they do not exceed the linear-in-coupling harmonic $\tilde{\xi}_{\pm\Delta\mathcal{R}}$ term. We take into account that in the τth dielectric half-space, the SPP electric field has predominantly a z component, and therefore, we replace $T^{\tau|-\sigma}_{\mathcal{R}}$ for $E^{\tau}_{\mathcal{R}z}$. It follows immediately from this system that the initial SPPs with wave vectors oriented at $\psi_{\mathcal{R}\mathcal{R}'}=\pm\pi/2$ are not coupled, and thus it is the instance where the quadratic coupling terms have to be retained.[63] Note that here the 2D problem is reduced to the 1D one that corresponds to the twofold SPP coupling through the harmonic grating of the period $2\pi/|\mathbf{k}_{R_1t}-\mathbf{k}_{R_2t}|$ (and with amplitude $\tilde{\xi}_{\pm\Delta\mathcal{R}}$), where the quasi-wave-vector of the dressed SPP, $\mathbf{q}$, and of the satellite, $\mathbf{q}'=\mathbf{q}+(r_1'-r_1)\mathbf{g}_1+(r_2'-r_2)\mathbf{g}_2$, refer to the sides of a Brillouin zone (see Fig. 2). Then, $\beta_{\tau|\mathcal{R}}=\beta_{\tau|\mathcal{R}'}\equiv\beta_\tau$, where $\beta_\tau=\sqrt{\varepsilon_\tau-(qc/\omega)^2}/\varepsilon_\tau$, and the dispersion relation becomes

$$\beta_\tau(\omega^{\pm})=-\xi_{\mathcal{O}}\mp\sqrt{\tilde{\xi}_{\Delta r}\tilde{\xi}_{-\Delta r}}|\cos\psi_{\mathcal{R}\mathcal{R}'}|. \quad (32)$$

It should be recalled that $\psi_{\mathcal{R}\mathcal{R}'}$ is the angle between $\mathbf{q}$ and $\mathbf{q}'$. Hence, we obtain the two roots: the first one is for the high-frequency mode ω^+ and the second one is for the low-frequency mode ω^-. Specifically, by neglecting the modulation of the small real part of the surface impedance as compared with that of its imaginary part, we have $\tilde{\xi}_{-m}=-\tilde{\xi}^*_m$, and

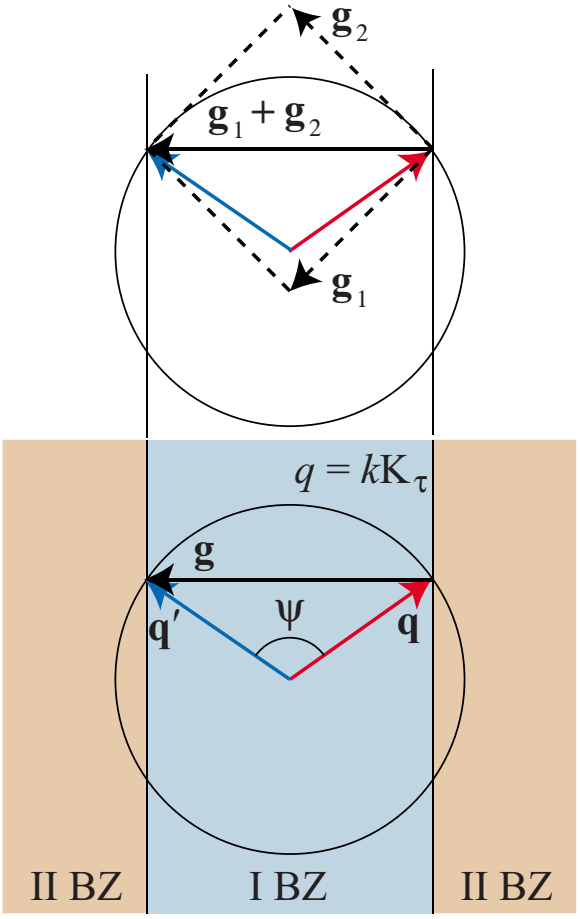

FIG. 2. (Color online) An example of a twofold coupling of the SPPs for $\Delta\mathcal{R}=(1,1)$. The top (bottom) figure is for the 2D (similar 1D) problem.

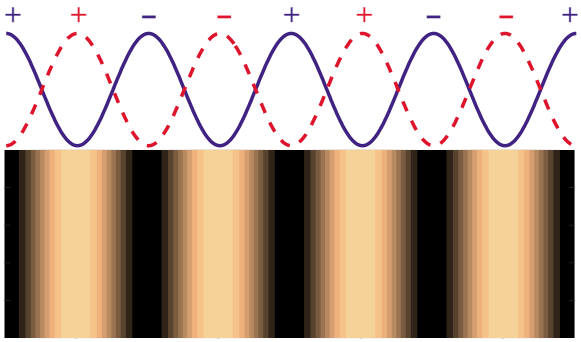

FIG. 3. (Color online) Spatial distribution of the squared electric field z components of the eigenmodes. The solid (dashed) curve is for the low- (high-) frequency mode. The "more metallic" regions of the coupling harmonic contribution are shown by the darker regions of the contour plot. Pluses and minuses refer to the signs of the surface charge density.

$\sqrt{\tilde{\xi}_{\Delta\mathcal{R}}\tilde{\xi}_{-\Delta\mathcal{R}}}=i|\tilde{\xi}_{\Delta\mathcal{R}}|$. Hence, the eigenfrequencies are

$$\omega^{\pm}/\omega_{ph} \simeq 1+\varepsilon_{\tau}\xi_{\mathcal{O}}^2/2 \pm i\varepsilon_{\tau}\xi_{\mathcal{O}}|\tilde{\xi}_{\Delta\mathcal{R}}\cos\psi_{\mathcal{R}\mathcal{R}'}|,$$

$$\omega_{ph}=qc/\sqrt{\varepsilon_{\tau}}, \tag{33}$$

where the upper (lower) sign is for high- (low-) frequency SPP. It is important to note that the quality (Q) factor for the high-frequency mode is higher than that for the low-frequency mode.

For the specific choice of coordinate origin, such that $\tilde{\xi}_{\Delta\mathcal{R}}=i|\tilde{\xi}_{\Delta\mathcal{R}}|$, $\xi(\mathbf{r}_t)=\xi_{\mathcal{O}}+\cdots+2i|\tilde{\xi}_{\Delta\mathcal{R}}|\cos[(\mathbf{q}-\mathbf{q}')\cdot\mathbf{r}]+\cdots$, the electric field amplitudes of the eigenmodes obey the relation $(E^{\tau}_{z\mathcal{R}}/E^{\tau}_{z\mathcal{R}'})^{\pm}=\pm\mathrm{sgn}[\cos\psi_{\mathcal{R}\mathcal{R}'}]$. As the coupled SPPs propagate in the opposite directions, $\psi=\pm\pi$, we get $\mathbf{q}=-\mathbf{q}'$, and the field structure at the interface for the eigenmodes is

$$E_z^{\tau(-)}(\mathbf{r}_t)\sim\cos(\mathbf{q}\cdot\mathbf{r}), \quad E_z^{\tau(+)}(\mathbf{r}_t)\sim\sin(\mathbf{q}\cdot\mathbf{r}). \tag{34}$$

Note that when the coupling in the first-order scattering is prevalent, or, in other words, with the coupling harmonic dominating over the others, $|\tilde{\xi}_{\Delta\mathcal{R}}|>|\tilde{\xi}_{\mathcal{M}}|^2$, the structure of the spatial field distribution is governed by the coupling harmonic. In other words, the field maxima of the high-frequency mode coincide with the "less metallic" regions (where $|\xi|$ is higher) relative to the coupling harmonic and vice versa for the low-frequency mode (see Fig. 3).

Now, let us examine the eigenmodes of the fourfold SB SPP resonance. We limit ourselves to $[r,0]$ resonance such that $\mathbf{k}_{(r,0)t}=-\mathbf{k}_{(-r,0)t}$, $\mathbf{k}_{(0,r)t}=-\mathbf{k}_{(0,-r)t}$, and $\mathbf{k}_{(0,\pm r)t}\perp\mathbf{k}_{(\pm r,0)t}$. Remember that the resonance amplitudes corresponding to perpendicularly oriented vectors are not coupled in the first scattering order. One can make sure that four eigenmodes exist. Two of them are "mixed," that is, all resonance amplitudes are nonzero: $E^{\tau}_{(\pm r,0)z}$, $E^{\tau}_{(0,\pm r)z}\neq 0$, and moreover, $E^{\tau}_{(r,0)z}=E^{\tau}_{(-r,0)z}$ and $E^{\tau}_{(0,r)z}=E^{\tau}_{(0,-r)z}$. Thus, the field structure has the form of the linear combination of two cosines having their periods along $\mathbf{g}_1$ and $\mathbf{g}_2$. These modes cannot be excited at normal incidence. Other two modes, which may be excited, have zero resonance amplitudes: for one mode $E^{\tau}_{(r,0)z}=-E^{\tau}_{(-r,0)z}$ and $E^{\tau}_{(0,\pm r)z}=0$, and for the other mode $E^{\tau}_{(0,r)z}=-E^{\tau}_{(0,-r)z}$ and $E^{\tau}_{(\pm r,0)z}=0$. Consequently, the spatial structure is specified by sinuses. Thus, the structure of the eigenmodes in this particular instance of fourfold SB SPP resonance is similar to that of twofold SB SPP resonances; they have the form of a pair of standing SPPs, which is appropriate to the sinus-type spatial field distribution, and higher-frequency (and also higher Q factor) branches. This means that in Eqs. (33) taking "+" we should set $|\cos\psi_{\mathcal{R}\mathcal{R}'}|\to 1$, $\Delta r\to(2r,0)$, and the first (second) standing SPP quasi-wave-vector $\mathbf{q}$ becomes parallel to $\mathbf{k}_{(r,0)t}$ [$\mathbf{k}_{(0,r)t}$].

The solution of the inhomogeneous problem is the superposition of the above standing SPPs with the "weights" proportional to cosines of the angles between $\mathbf{H}^{\tau}_{(r,0)t}$, $\mathbf{H}^{\tau}_{(0,r)t}$, and $\mathbf{H}$. The eigenmodes for other SB fourfold resonances may be treated in a similar way: they are the combinations of the simplest SPP modes as well.

The field structure of DB dressed SPPs is defined by the coupling of the initial SPPs both through the modulation and through the finite film thickness. The field structure resulting from the coupling through the film thickness may be understood from the example of the undressed SPP existing in the unmodulated film. The eigenfrequencies for this instance are defined by Eq. (17). Note that in contrast to the dielectric half-spaces, the amplitude of the tangential-to-interface component of the electric field inside the metal is higher than the z component, $|\bar{E}_t/\bar{E}_z|\sim|\sqrt{\varepsilon}|\gg 1$. Remind also that the z dependence of the electric field inside the film for LR and SR eigenmodes is[1,2]

$$\bar{E}_t^{(L)}\sim\sinh(\tilde{k}z-\Phi/2), \quad \bar{E}_t^{(S)}\sim\cosh(\tilde{k}z-\Phi/2), \tag{35}$$

where (L) stands for LR SPP and (S) for SR SPP.

For dressed DB SPPs with the twofold coupling, the dispersion relations are

$$\beta^{(L\pm)}=-(\xi_{\mathcal{O}}\pm\tilde{\xi}_{\Delta\mathcal{R}}|\cos\psi|)\tanh(\Phi/2),$$

$$\beta^{(S\pm)}=-(\xi_{\mathcal{O}}\pm\tilde{\xi}_{\Delta\mathcal{R}}|\cos\psi|)\coth(\Phi/2), \tag{36}$$

where $\beta^{(\cdots)}=\sqrt{\varepsilon_d-(qc/\omega)^2}/\varepsilon_d$, $\varepsilon_+=\varepsilon_-=\varepsilon_d$, and the superscripts in brackets mark the eigenmodes. Here, the initial SPPs (and their diffraction indexes) are the same as those forming the dressed twofold SB SPP. The spatial field distribution of eigenmodes inside the film for $\psi=\pi$ ($\mathbf{q}=-\mathbf{q}'$) has the form

$$\bar{\mathbf{E}}_t^{(S-)}(\mathbf{r})\sim\hat{\mathbf{e}}_{\mathbf{q}}\cosh(\tilde{k}z-\Phi/2)\sin(\mathbf{q}\cdot\mathbf{r}),$$

$$\bar{\mathbf{E}}_t^{(L-)}(\mathbf{r})\sim\hat{\mathbf{e}}_{\mathbf{q}}\sinh(\tilde{k}z-\Phi/2)\sin(\mathbf{q}\cdot\mathbf{r}),$$

$$\bar{\mathbf{E}}_t^{(S+)}(\mathbf{r})\sim\hat{\mathbf{e}}_{\mathbf{q}}\cosh(\tilde{k}z-\Phi/2)\cos(\mathbf{q}\cdot\mathbf{r}),$$

$$\bar{\mathbf{E}}_t^{(L+)}(\mathbf{r})\sim\hat{\mathbf{e}}_{\mathbf{q}}\sinh(\tilde{k}z-\Phi/2)\cos(\mathbf{q}\cdot\mathbf{r}). \tag{37}$$

The z components of the electric field in the dielectrics at the film faces are of the same form as in Eq. (34), i.e.,

$E_z^{\tau(S-)}(\mathbf{r}) \sim E_z^{\tau(L-)}(\mathbf{r}) \sim \cos(\mathbf{q}\cdot\mathbf{r})$ and $E_z^{\tau(S+)}(\mathbf{r}) \sim E_z^{\tau(L+)}(\mathbf{r}) \sim \sin(\mathbf{q}\cdot\mathbf{r})$. It is possible to obtain the eigenfrequencies and the field structure for the fourfold DB SPP, proceeding in the same way, in which we generalized the twofold SB SPP to the fourfold SB SPP.

Analyzing the denominator of TCs, one can make certain that the excited DB SPPs are related to + modes only. Indeed, with the film thickness tending to infinity, we see that the two poles of TCs in Eq. (B1) of Appendix B, $\Delta_{\mathcal{R}}=0$, become $\beta_{\tau|\mathcal{R}}+\xi_{\mathcal{O}}+\tilde{\xi}_{2\mathcal{R}}=0$, when neglecting the second-order scattering processes. Choosing an origin such that $\tilde{\xi}_{2\mathcal{R}} = i|\tilde{\xi}_{2\mathcal{R}}|$, the poles coincide with the + branch of Eq. (32), where $\tilde{\xi}_{2\mathcal{R}}$ is replaced by $\tilde{\xi}_{\Delta\mathcal{R}}$ and $|\cos\psi_{\mathcal{R}\mathcal{R}'}|=1$. This corresponds to the upper frequency branch [Eq. (33)] and, hence, to the "sine" field distribution in the x-y plane.

Under the assumption of C_{4v} modulation symmetry, the zeroth-order TCs for SB $[r,0]_\tau$ resonance have the structure similar to Eq. (29) as well (see Appendix B). However, the difference is that identity $T_{\mathcal{O}}^{\tau|\sigma\bar{\sigma}}=0$ holds, which ensures that the polarization of the zeroth-order transmitted wave coincides with that of the incident wave.

Along with the anomalies resulting from SPP excitation, there exist Rayleigh anomalies. They are related to the boundary between homogeneous (propagating) and inhomogeneous (evanescent) waves in different diffraction orders, viz., to the vanishing of the z component of one of the wave vectors, $k_{\tau|\mathcal{M}z}=0$, or $\beta_{\mathcal{M}|\tau}=0$. Mathematically, the Rayleigh anomalies are the branch points; they give rise to the discontinuity of the incident angle or wavelength derivative of the transformation coefficients. In what follows, we will denote the Rayleigh anomalies as $(m_1,m_2)_\tau^R$ (which points out to the vanishing of $\beta_{\tau|m_1,m_2}$) or as $[m_1,m_2]_\tau^R$ (this indicates the vanishing of $\beta_{\tau|[m_1,m_2]}$).

Since modulation harmonics play a crucial role in SPP excitation, let us consider in the following section the Fourier representation of the structures widely used in the experiments.

D. Modulation spectra

Most of experimental works deal with hole arrays in metal films deposited onto a dielectric substrate (predominantly onto quartz) (see Fig. 1). Instead of holes, we will consider cylindrical inclusions in the film. The inclusions are supposed to consist of a metal or a semiconductor with the dielectric permittivity different from that of the film. Both the inclusions and the film must be highly conducting. As seen below, this structure may qualitatively describe the optical properties of nanohole arrays, even though the film does not contain holes as such. Furthermore, the results from our studies may be used to model and describe the arrays of cylindrical nanoparticles, so far examined experimentally. Indeed, the structure considered may be fabricated by making an array of cylindrical nanoparticles with impedance ξ_i, which are inserted into a conducting film.

For the inclusions of a round cross section with radius a, we have

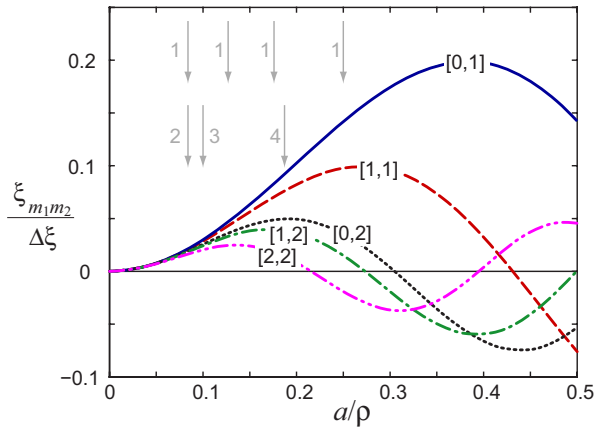

FIG. 4. (Color online) Modulation harmonics ξ_{m_1,m_2} dependence on the ratio of the cylindrical inclusion radius to the period of the square array, a/ρ. Arrows 1, 2, 3, and 4 indicate a/ρ values of the hole arrays examined in Refs. 5, 6, 14, and 9, respectively.

$$\tilde{\xi}_{\mathcal{M}} = \frac{2\pi a\Delta\xi}{\Sigma\cdot g_{\mathcal{M}}} J_1(ag_{\mathcal{M}}), \quad \xi_{\mathcal{O}} = \xi_f + \frac{\pi a^2\Delta\xi}{\Sigma},$$

$$\mathbf{g}_{\mathcal{M}} = m_1\mathbf{g}_1 + m_2\mathbf{g}_2, \quad \Sigma = |\boldsymbol{\rho}_1 \times \boldsymbol{\rho}_2|, \tag{38}$$

where $\Delta\xi=\xi_f-\xi_i$ is the difference between the film (ξ_f) and the inclusion (ξ_i) surface impedance, and J_1 is the first-order Bessel function. A typical example for the Fourier spectrum of the array of cylindrical inclusions for the square symmetry structure is shown in Fig. 4. The square symmetry structure implies that the angle between translation vectors is $\pi/2$ and their modules are equal, $\rho_1=\rho_2$. In the following calculations, we take ξ_f to be equal to the impedance of Ag (using the wavelength dependence from Ref. 64); the impedance of inclusions will be modeled as $\xi_i=w\xi_f$, where w is a dimensionless parameter.

As seen from Eq. (24), the amplitude of the resonance ($\mathcal{R}$th) diffraction order is proportional to $\tilde{\xi}_{\mathcal{R}}$, $H_{\mathcal{R}}^{\tau|\sigma} \propto \tilde{\xi}_{\mathcal{R}}$; therefore, the efficiency of SPP excitation in this order is strongly dependent on the "resonance" amplitude $\tilde{\xi}_{\mathcal{R}}$. For large values of r_1, r_2, the Fourier amplitude $\tilde{\xi}_{\mathcal{R}}$ tends to zero as

$$\tilde{\xi}_{\mathcal{R}} \sim g_{\mathcal{R}}^{-3/2}, \quad |\mathcal{R}| \gg 1. \tag{39}$$

Thus, the resonances in high diffraction orders are less efficient. If the inclusion diameter is far smaller than the modulation periods, the low-order amplitudes are approximately independent of their order:

$$\tilde{\xi}_{\mathcal{M}} \simeq \pi\Delta\xi a^2\Sigma^{-1}[1+O(ag_{\mathcal{M}})] \quad \text{for } ag_{\mathcal{M}} \ll 1. \tag{40}$$

So, for very thin inclusions the Fourier amplitudes of the structure decrease slightly when $|\mathcal{M}|$ decreases, which is valid for an arbitrary cross section of the inclusions. In its turn, it significantly broadens the SPP resonances: they become "diffusive" due to equal contribution from many scattering processes of the excited SPPs.

Also, we give the Fourier expansion of the structure having the inclusions of a rectangular cross section as

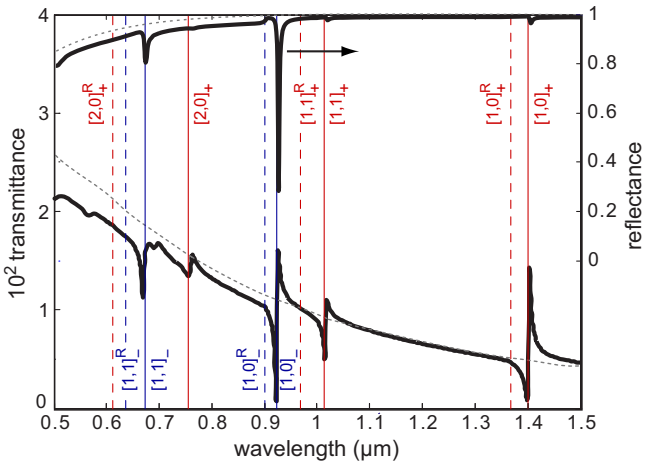

FIG. 5. (Color online) Wavelength-dependent transmittance and reflectance for the normal incidence from the air superstrate onto the silver film bounding with the quartz substrate. The parameters of the C_{4v} array are $\rho_1=\rho_2=\rho=0.9$ μm and $a/\rho=1/3$. The incident-wave electric field $\mathbf{E}$ is parallel to $\mathbf{g}_1$ (to the Ox axis, see Fig. 1). The inclusion impedance ξ_i is taken to be $\xi_i=2\xi_f$. The film thickness is equal to 2.3 skin depths. The transmittance and reflectance of the unmodulated film are plotted with dotted lines. The vertical solid and dashed lines indicate the wavelengths relevant to SPPs on the unmodulated boundaries and Rayleigh points, respectively.

$$\tilde{\xi}_{\mathcal{M}} = \frac{4a_1a_2\Delta\xi}{(\mathbf{a}_1\cdot\mathbf{g}_{\mathcal{M}})(\mathbf{a}_2\cdot\mathbf{g}_{\mathcal{M}})\Sigma}\sin\frac{\mathbf{a}_1\cdot\mathbf{g}_{\mathcal{M}}}{2}\sin\frac{\mathbf{a}_2\cdot\mathbf{g}_{\mathcal{M}}}{2}, \tag{41}$$

where $\mathbf{a}_{1,2}$ are the vectors oriented along the sides of the rectangular inclusions with modulus equal to their lengths, $a_{1,2}$.

III. SB SPP RESONANCES: NONSYMMETRIC SURROUNDING

Bearing in mind the experiments, periodically modulated films surrounded by two different dielectric media are of special interest. These structures can support both SB SPPs and, under the special conditions, DB SPPs. The latter will be discussed separately. In the vicinity of normal incidence that we mainly focus on, the resonances are basically related to SBSPPs. An example of the transmittance and reflectance wavelength spectra at strictly normal incidence is illustrated in Fig. 5. The calculations are for the C_{4v} array of inclusions with a round cross section in the Ag film surrounded by air superstrate and quartz substrate. The transmittance and reflectance extremes are pronounced at wavelengths for the SPPs existing at unmodulated metal-quartz and metal-air interfaces. Note that while the extremes are shifted with respect to initial SPPs wavelength, which is due to the modulation and finite film thickness influence, Rayleigh anomalies are unshifted.

Now, we discuss the vicinity of the strictly normal incidence. In Figs. 6(a)–6(c) and 6(e), the transmittance contour plot is shown as a function of the wavelength or/and photon energy and the incident angle for different polarizations of the incident wave. In Figs. 6(d) and 6(f), the resonance curves (18) corresponding to the contour plots in Figs. 6(a)–6(c) are shown. The transmittance features and the resonance curves show an excellent agreement. It should be emphasized that there is a strong dispersion, $\xi(\lambda)$, in the short-wavelength region. In Figs. 6(a)–6(c), the special symmetry instances are given, viz., the coincidence of the resonance curves is due to the orientation of the incident plane relative to one of the reciprocal grating vectors ($\mathbf{g}_1$) at angles 0 (or $\pi/2$) and $\pi/4$ [see discussion below formula (18)]. The coincidence is noticeable in the vicinity of $[1,0]_+$, $[1,1]_+$, and $[1,0]_-$ resonances. In Fig. 6, these vicinities are marked by squares. We see that in Figs. 6(a)–6(c), one to three resonance features belong to these regions. Respectively, in Figs. 6(d) and 6(f), one to three resonance curves intersect these regions. Alternatively, four resonance "mountain ridges" intersect in the vicinity of a single point [see Fig. 6(e)], which illustrates the transmittance contour plot for the nonspecific value of angle ψ.

Note that the intersections of solid and dashed resonance curves in Figs. 6(d) and 6(f) and the intersections of corresponding resonance mountain ridges in the transmittance contour plots are due to DB SPP resonances. The latter comply with the excitation of dressed SPPs, resulting from the coupling of initial SPPs of different film faces through the modulation.

In the following sections, we examine in detail some of SB fourfold resonances.

A. $[1,0]_+$ resonance

Consider first the longest-wavelength resonance (at 1.4 μm in Fig. 5) in the vicinity of close-to-normal incidence. This resonance arises due to excitation of the fourfold $[1,0]_+$ SB SPP at the metal-quartz interface with C_{4v} modulation symmetry.

In Figs. 7(a) and 7(c), the enlarged fragments of Figs. 5 and 6(a) are shown in the vicinity of $[1,0]_+$ resonance for the incident plane orientated parallel to $\mathbf{g}_1$ and the polarization of the incident wave such that $\mathbf{E}\|\mathbf{g}_1$. Note that the resonance features are heavily dependent on the polarization of the incident wave and the orientation of the incident plane [see transmittance dependences shown in Figs. 6(a)–6(c) and 6(e)]. For instance, for p polarization, when $\mathbf{E}$ belongs to the incident plane parallel to $\mathbf{g}_1$ ($\psi=0$), in the vicinity of normal incidence, only the pair of the resonance waves are excited (see Sec. II C). These waves are of $(\pm1,0)$ diffraction orders (although TCs $T_{0,\pm1}^{+|--}$ are equal to zero). In Figs. 6(a) and 7(a), one can observe the intersection of the two resonance features relevant to $(1,0)_+$ and $(-1,0)_+$ resonance curves in Fig. 6(d). In deflecting from the normal incidence, the projection of $\mathbf{H}_t$ onto $\mathbf{H}_{0,\pm1}^+$ becomes nonzero, and it reveals itself as a feature in Fig. 6(a) close to the coinciding resonance curves $(0,\pm1)_+$ in Fig. 6(d). When $\mathbf{E}$ is perpendicular to the incident plane parallel to $\mathbf{g}_1$ ($\psi=0$) [s polarization, see Fig. 6(b)], the only excited pair of resonance waves comply with the diffraction orders $(0,\pm1)$ (resonance coefficients $T_{0,\pm1}^{+|--}$). If the incident plane is oriented at $\psi\neq0$, $\pi/4$, then two pairs of resonance waves are excited both for p and s polarizations of

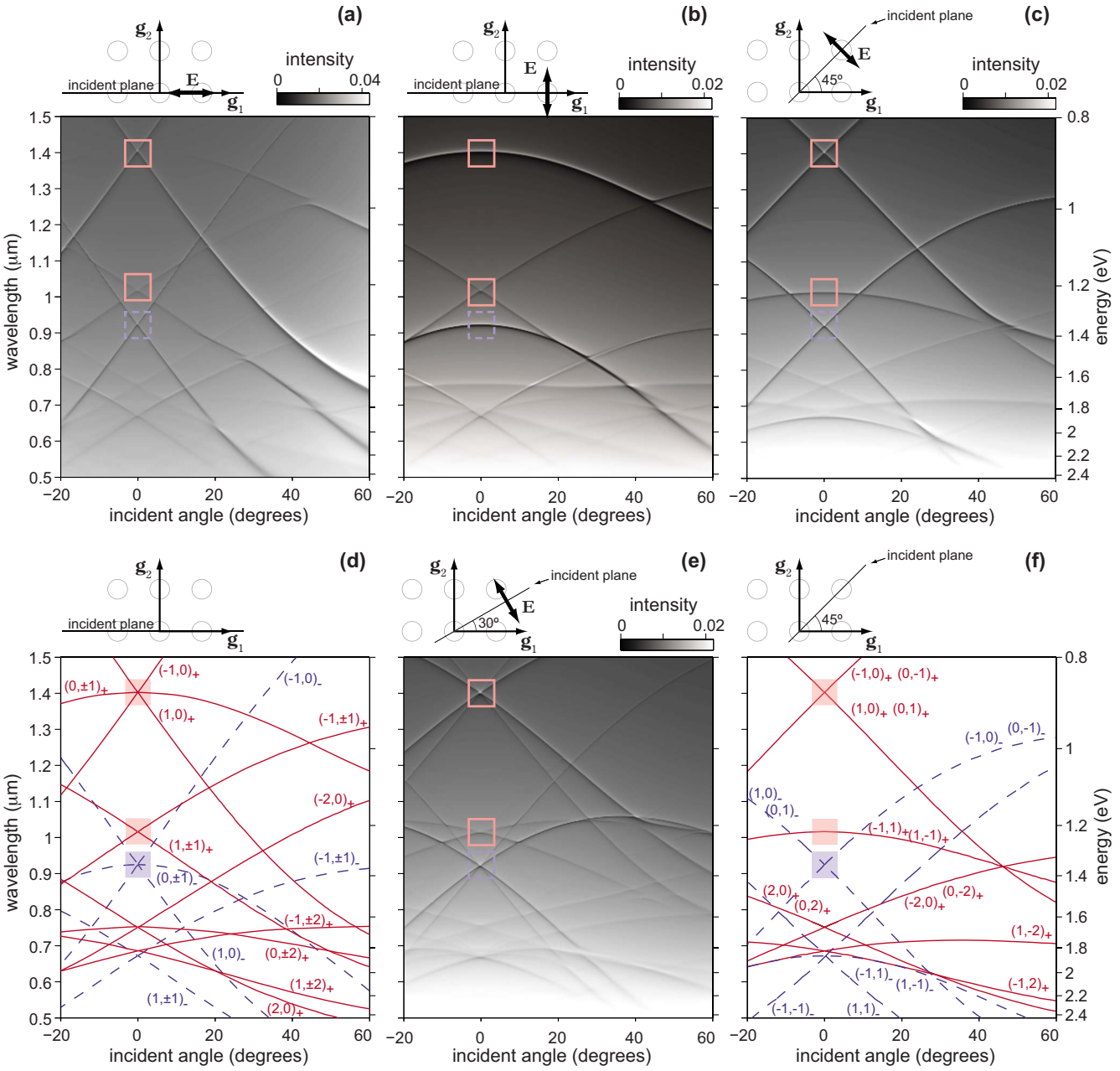

FIG. 6. (Color online) Dependence of transmittance on the wavelength (energy) and the incident angle for different polarizations of the incident wave and different orientations of the incident plane. The array and the film parameters are the same as in Fig. 5. In (d) and (f), solid and dashed lines are the resonance curves [Eq. (18)]. Solid (dashed) squares indicate the vicinity of the quartz-silver (air-silver) resonances which are discussed in detail in the text.

the incident wave in the vicinity of normal incidence [in Figs. 6(c)–6(e), the *s*-polarization case is shown]. The resonance waves are of diffraction orders $(\pm 1, 0)$ and $(0, \pm 1)$ and their dispersion branches in the form of four resonance curves $[(\pm 1, 0)_+$ and $(0, \pm 1)_+$ coinciding for $\psi = \pi/4]$ intersect, as seen in Fig. 6(f).

The wavelength dependence of the zeroth-order wave has the typical Fano-type profile which consists of the neighboring minima and maxima [see Fig. 7(c)]. This is due to the interference (see Sec. II B) between nonresonance and resonance transmittance mechanisms. The maxima of the Fano profile are red shifted as compared with the wavelength of the SPP existing at the nonmodulated metal-quartz interface. This shift is mainly due to the scattering by modulation through the diffracted inhomogeneous waves, and partially due to the finite film thickness.

The amplitude of the excited resonance waves is proportional to $\tilde{\xi}_{[10]}$ Fourier harmonic amplitude, while the zeroth-order transmittance and reflectance are proportional to its squared value, as it follows from Eqs. (24)–(30) (see also Appendix B). Therefore, this harmonic plays the most important role in the excitation of the SPP eigenmode for $[1, 0]_+$ resonance. Actually, the structure of the eigenmodes in the modulated film (dressed SPPs) defines the distribution of the

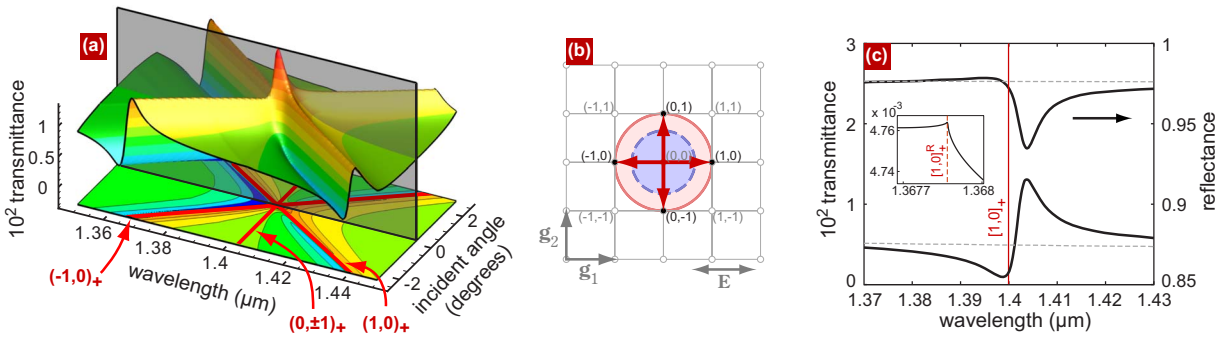

FIG. 7. (Color online) (a) The dependence of the zeroth-order transmittance $\tau_{\mathcal{O}}$ on the wavelength and the incident angle in the vicinity of the $[1,0]_+$ resonance on a silver array of inclusions with symmetry C_{4v} for $\mathbf{E}\|\mathbf{g}_1$. In (b), the reciprocal grating is shown, where the radii of solid and dashed circles are equal to the SPP wave vector modulus in quartz and air half-spaces, respectively; the circles separate the regions of propagating (filled area) and evanescent waves in the superstrate and substrate. In (c), the wavelength dependence for the zeroth-order transmittance $\tau_{\mathcal{O}}$ and reflectance $\rho_{\mathcal{O}}$ are shown, which belong to the gray section in (a). The inset shows the vicinity of the Rayleigh anomaly. The parameters of the array are the same as in Fig. 5.

near field completely. As indicated in Sec. II C, only high-frequency eigenmodes are excited. For instance, when $\mathbf{E}$ is oriented along $\mathbf{g}_1$, the distribution of the squared field on the quartz side takes the form $|\mathbf{E}^+|^2 \sim \sin^2[\mathbf{k}_{(1,0)t}\cdot\mathbf{r}] = \sin^2(\mathbf{g}_1\cdot\mathbf{r})$ similar to the spatial field distribution for the twofold coupling given by Eq. (34). Indeed, this is in compliance with the left-hand part of Fig. 8(a). In the general case, when $\mathbf{E}$ is oriented relative to $\mathbf{g}_1$ at an arbitrary angle ψ, the near-field structure is formed by the interference of the eigenmodes. One of them corresponds to $\sin(\mathbf{g}_1\cdot\mathbf{r})$ and the other is for $\sin(\mathbf{g}_2\cdot\mathbf{r})$. As a result, the field of the interface is expressed as $|\mathbf{E}^+|^2 \sim [\chi_1 \sin(\mathbf{g}_1\cdot\mathbf{r}) + \chi_2 \sin(\mathbf{g}_2\cdot\mathbf{r})]^2$, where the weight coefficients χ_1 (χ_2) are proportional to $\cos\psi$ ($\sin\psi$). This interference is clearly seen in the right-hand part of Fig. 8(a). Thus, the near-field structure is in good agreement with the experiment (see Ref. 14).

Consider the field distribution along the z axis [Fig. 8(b)]. Since the far-side SB SPP resonances provide small reflectance dips [the lowest reflectance is of order of 93%, see Fig. 7(c)], we notice an interference pattern along the z axis in the air half-space. The field penetrating into the film decays exponentially and excites a SB SPP at the quartz-metal interface. The SPP field has a well-pronounced "torch" structure. It decays exponentially into the film at a distance of order of skin depth δ, where $\delta/\lambda \sim 1/|\sqrt{\bar{\varepsilon}}| \ll 1$, and decays into the dielectric medium (quartz) at a distance of δ_+, where $\delta_\tau/\lambda \simeq \sqrt{|\bar{\varepsilon}/\varepsilon_\tau|}/2\pi \sim 1$. Note that the field pattern along the x axis in the film is shifted to a half-period with respect to the pattern in the quartz. This is because the SPP electric field in the metal has predominantly tangential-to-interface component as compared with a dielectric where the electric field has predominantly normal-to-interface component. The intensity of the far field in the quartz half-space is constant, since there exists only one propagating wave (at zeroth diffraction order).

B. Polarization properties of $[1,0]_+$ resonance: Dependence on the inclusion shape

In this section, we give a theoretical interpretation of the recent experiments[39,41] with the influence of the hole shape

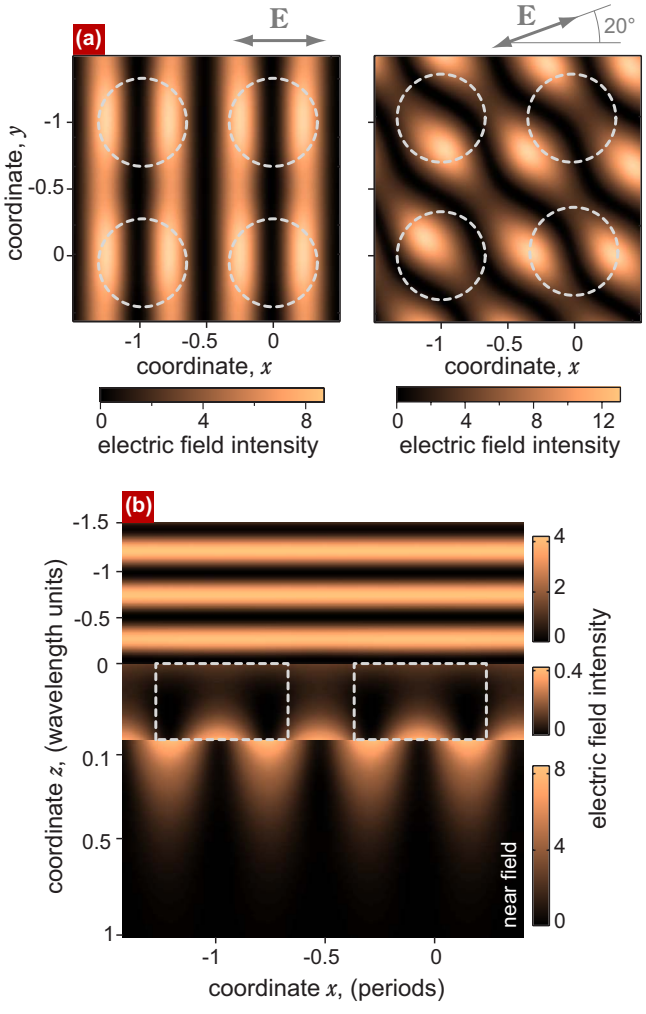

FIG. 8. (Color online) The squared field distribution is shown for the $[1,0]_+$ SPP resonance at $\lambda = 1.4023$ μm, $\theta = 0$. The inclusions are shown by the dashed lines. The parameters of the array are the same as in Fig. 5.

on ELT through periodic hole arrays within the framework of our theory. Moreover, we describe the transmittance behavior while changing the polarization of the incident light.

Consider a silver film sandwiched between an air superstrate and a quartz substrate with C_{2v} modulation symmetry resulting from the rectangular cross section of the inclusions. This symmetry reduces to C_{4v} symmetry for a circular cross section of inclusions. Now, let us scrutinize the $[1,0]_+$ SB fourfold SPP resonance at strictly normal incidence. As was discussed above, for C_{2v} symmetry structures the polarization of the transmitted radiation depends on the polarization of the incident wave. Suppose that the direction of $\mathbf{g}_1$ is parallel to the small side of the rectangular cross section, a_1. If the incident-wave electric field is oriented along $\mathbf{g}_1$ [$\mathbf{g}_2$], the incident-wave magnetic field is then matched with that of $(\pm 1,0)_+$ [$(0,\pm 1)_+$] SPP pairs having wave vectors $\pm\mathbf{g}_1$ [$\pm\mathbf{g}_2$] for normal incidence [see Fig. 7(b)]. According to our approach, the transmittance coefficient $\tau_{\mathcal{O}}$ is proportional to $\tilde{\xi}^4_{\pm 1,0}$ ($\tilde{\xi}^4_{0,\pm 1}$) with a polarization along $\mathbf{g}_1$ ($\mathbf{g}_2$). This leads to $\tau_{\mathcal{O}} \sim (\Delta\xi)^4 (a/\rho)^4 J_1^4(2\pi a/\rho)$ for circular cross section and $\tau_{\mathcal{O}} \sim (\Delta\xi)^4 (a_2/\rho)^4 \sin^4(\pi a_1/\rho)$ [$\tau_{\mathcal{O}} \sim (\Delta\xi)^4 (a_1/\rho)^4 \sin^4(\pi a_2/\rho)$] for rectangular cross section with **E** orientation along $\mathbf{g}_1$ ($\mathbf{g}_2$) [see Eqs. (38) and (41)]. We take the same geometrical parameters for periodic arrays as in Ref. 39, i.e., ρ=425 nm, $a_1 \times a_2 = 75 \times 225$ nm^2 for small rectangles and $a_1 \times a_2 = 150 \times 225$ nm^2 for large ones, and $2a$=190 nm for the circle diameter which corresponds to the resonance position at $\lambda \simeq 0.72$ μm. Assuming the film thickness to be equal to 3 skin depths, $\Phi'=3$, and the inclusion impedance to be $\xi_i = 2\xi_f$, where ξ_f is taken for the silver, we obtain the transmittance of order 2%, which is nearly seven times higher than the transmittance through the unmodulated film.

When **E** is directed along $\mathbf{g}_1$, the zeroth-order transmittance amplitude is proportional to a squared $\tilde{\xi}_{\pm 1,0}$ harmonic amplitude. This amplitude increases for large rectangles as compared with the circles and this results in a redshift and in a rise of the transmittance maximum [see Fig. 9(a)]. This tendency agrees with the experiment. However, for the small rectangles the resonance harmonic amplitude is the smallest one and this leads to a blueshift and a decrease in the transmittance maxima as compared with the circles and large rectangles. This is not what was observed experimentally. We may eliminate this discrepancy only by adjusting the impedance of the inclusion. We use this adjustment because, in our approximation, we do not allow for the influence of the modulation on the volume of the film, but the modulation appears in the boundary conditions only. In other words, the fields decay into the film with the same decrement at any cross section by a plane parallel to axis Oz. On the other hand, it is evident that under a strong modulation, with the impedances of inclusions and the film differing greatly, the fields in the inclusion and in the volume of the film decay in a different way. For instance, inside the holes the field show a weaker decay than in the metal regions. Thus, adjusting the impedance, we have found that for $\xi_i > 2.67\xi_f$ the transmittance maximum corresponding to the small rectangles is redshifted and increased as compared with the large rectangles and circles as it was in the experiment. If we rotate the polarization plane by $\pi/2$ so that **E** is directed along $\mathbf{g}_2$ [see Fig. 7(b)], the transmittance will depend on the inclusion shape in a different manner. In Fig. 9(b), the transmittance is shown for different inclusion shapes both with equal ξ_i for all shapes and when the modulation amplitude is taken from the previous case for the small rectangles.

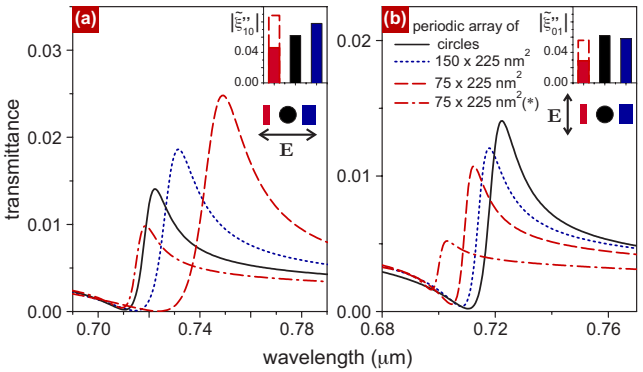

FIG. 9. (Color online) The wavelength dependence of transmittance for the inclusion with different cross sections at strictly normal incidence onto the Ag film deposited onto the quartz substrate. The polarization of the incoming light **E** is perpendicular to the long axis of the rectangles in (a) and parallel to the long axis of the rectangles in (b). The dotted curves are for the large rectangular inclusions. The dashed and dash-dotted curves are for the small rectangular inclusions. The solid curves correspond to the cylindrical inclusions. The film thickness is equal to 3 skin depths. In the insets, the amplitudes of the $(\pm 1,0)$ and $(0,\pm 1)$ modulation harmonics are shown. The dashed rectangular area in the insets indicates the modulation amplitude of $(0,\pm 1)$ harmonics for the dashed curve, for which $\xi_i = 3\xi_f$.

On the one hand, supposing the inclusion impedance ξ_i to be constant, but at the same time changing the inclusion shape, we can predict the true transmittance through arrays of nanoparticles immersed into the film (each nanoparticle corresponds to an inclusion). On the other hand, by adjusting the inclusion impedance for different shapes, we may provide the qualitative coincidence with experimental measurements of ELT through hole arrays.

Consider the experiment of Ref. 41, where the effect of aspect ratio of rectangular holes on the transmittance of periodic arrays of subwavelength holes in optically thick metal films was measured. It was found that as the electric field **E** of the incident light is directed along the short axes of the holes, a_1, the zeroth-order transmittance peak (corresponding to the $[1,0]_+$ SPP resonance) increases and suffers a redshift when the aspect ratio of the holes, a_2/a_1, is enlarged. Conversely, it was discovered that as **E** is directed along the long axes of the holes, a_2, the $[1,0]_+$ transmittance peak decreases and undergoes a blueshift when the aspect ratio of the holes is enlarged. The experimental measurements were also confirmed by strict numerical calculations. The authors attribute the discovered polarization dependence of the transmittance on the ratio of the rectangular holes to a result from interaction between SPP resonances at the surface of the metal and shape resonances inside the holes.

We hold to a different, simpler point of view. It is obvious that the localized eigenmodes are not supported by the struc-

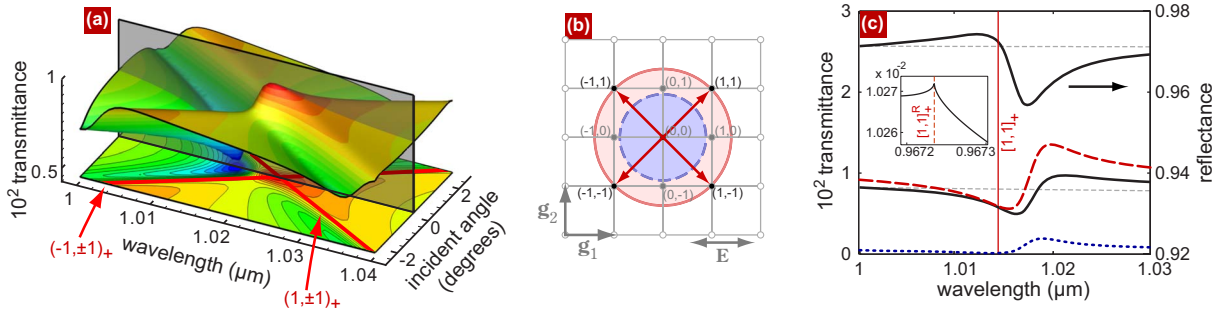

FIG. 10. (Color online) (a) The dependence of the zeroth-order transmittance $\tau_{\mathcal{O}}$ on the wavelength and incident angle corresponding to the $[1,1]_+$ resonance on a C_{4v} silver array of cylindrical inclusions, $\mathbf{E}\|\mathbf{g}_1$. In (b), the reciprocal grating is shown [compare with Fig. 7(b)]. In (c), the wavelength dependence for the zeroth-order transmittance $\tau_{\mathcal{O}}$ and reflectance $\rho_{\mathcal{O}}$ (solid curves) along with the nonzeroth-order transmittance $\tau_{(\pm1,0)}$ (dotted curve) and total transmittance τ_{tot} (dashed curve) are shown. It corresponds to the section in (a) along the plane, marked in gray. The inset presents the Rayleigh anomaly. The parameters of the array are the same as in Fig. 5.

tures under examination. However, the calculations we do not present here within the framework of our simple model exhibit the same behavior of the transmittance, as in Ref. 41. We have taken the geometrical parameters of the inclusions the same as in Ref. 41. When **E** is parallel to a_1, the amplitude of the excited $(\pm1,0)_+$ SPP is proportional to $\tilde{\xi}_{\pm1,0}$, which increases as the aspect ratio increases. Therefore, this leads to the transmittance peak growth and redshift. On the contrary, when **E** is parallel to a_2, the amplitude of the excited $(0,\pm1)_+$ SPP is proportional to $\tilde{\xi}_{0,\pm1}$, which decreases with an increasing aspect ratio. This brings about the transmittance peak decrease and blueshift. Thus, the polarization behavior may be successfully described under the assumption of the excitation of purely interface SPPs.

C. $[1,1]_+$ resonance

Now, examine the resonance near 1 μm (1.65 eV) in the vicinity of close-to-normal incidence (see Figs. 5 and 6). This fourfold $[1,1]_+$ resonance is consistent with excitation of a SB SPP at the metal-quartz interface [see Fig. 10(b)]. λ-θ dependence is shown in Fig. 6 (square regions) for different polarizations and orientations of the incident plane. Figures 10(a) and 10(c) are the enlarged fragments of Figs. 6(a) and 5.

Let us focus on the dependence of the transmittance on λ and θ in the vicinity of the $[1,1]_+$ resonance [see the second (from above) solid square regions in Fig. 6]. For *p* polarization, when **E** belongs to the incident plane parallel to $\mathbf{g}_1$ ($\psi=0$), both the pairs of the resonance waves corresponding to $(\pm1,\pm1)$ and $(\mp1,\pm1)$ diffraction orders are excited in the close-to-normal incidence region. Accordingly, in Figs. 6(a) and 10(a), one can see the intersection of the two features that are relevant to two pairs of coinciding resonance curves, $(1,\pm1)_+$ and $(-1,\pm1)_+$, in Fig. 6(d). Obviously, similar dependences take place if **E** is perpendicular to the incident plane parallel to $\mathbf{g}_1$ ($\psi=0$) [*s* polarization, see Fig. 6(b)]. If the incident plane is oriented at $\psi=\pi/4$, then for *s* polarization of the incident wave [see Fig. 6(c)] the magnetic field **H** is parallel to $\mathbf{g}_2-\mathbf{g}_1$, and the only excited pair of resonance waves in the vicinity of normal incidence corresponds to the diffraction orders $(\pm1,\mp1)$ (resonance coefficients $T^{+|--}_{\pm1,\mp1}$). This pair provides an extremum of the transmittance close to the coinciding resonance curves $(\pm1,\mp1)_+$ in Fig. 6(f). For the nondegenerated case ($\psi=30°$) [Fig. 6(e)], there is the intersection of four features in the transmittance which conforms to four distinct resonance curves: $[1,1]_+$.

The principal difference of the $[1,1]_+$ resonance from the $[1,0]_+$ resonance considered above is that additional propagating waves exist in the quartz substrate. In other words, the waves having [1,0] diffraction orders provide the nonzeroth-order ELT[31,32] due to the scattering of the resonance waves through amplitudes $\tilde{\xi}_{[1,0]}$. This scattering contributes additionally to the resonance width. Black dots, placed within the solid circle in Fig. 10(b), indicate the positions for tangential components of wave vectors of these waves. On the other hand, the resonance $[1,1]_+$ is less pronounced as compared with the $[1,0]_+$ one not only because of additional radiation losses. As seen in Fig. 4, the amplitude $\tilde{\xi}_{[1,1]}$, which is responsible for resonance wave excitation within the limits of the main approximation, is smaller than amplitude $\tilde{\xi}_{[1,0]}$, and hence, the SPP excitation is less effective. It should be noted that the SPP is excited not only owing to first-order scattering of the incident wave by [1,1] resonance harmonics but also due to the higher-order scattering processes. While the cubic processes (proportional to $\tilde{\xi}^3$) can be neglected, the second-order scattering may compete with the linear one in some regions of parameter a/ρ, going beyond approximations (19)–(22). Thus, for $a/\rho>0.35$, the contribution to the amplitude of the resonance wave from the second-order term, proportional to $\tilde{\xi}^2_{[1,0]}$, is of the the same order as the contribution from the linear term proportional to $\tilde{\xi}_{[1,1]}$.

All the propagating field harmonics contribute to the transmitted energy flux in the substrate media. Although the parts of the energy flux relating to the zeroth and nonzeroth diffraction orders are well separated at a great distance from the film, they overlap in the region sufficiently close to the film. Therefore, when making the experimental measurements, the detector position is crucial: if it is far away from the film, it fixes either zeroth-order flux, $\tau_{\mathcal{O}}$ [see Fig. 10(c),

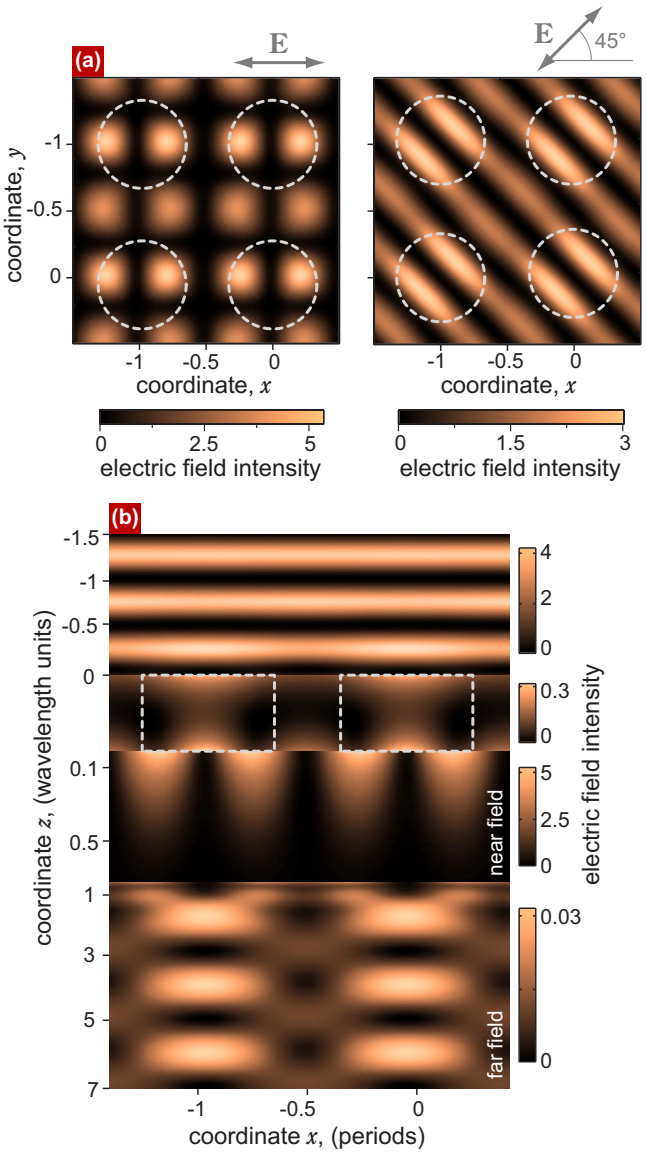

FIG. 11. (Color online) The squared field distribution for the $[1,1]_+$ SPP resonance is shown at $\lambda=1.0168$ μm, $\theta=0$. The parameters of the array are the same as in Fig. 5.

solid curve], or nonzeroth one, $\tau_{[1,0]}$ [see Fig. 10(c), dotted curve], depending on detector orientation relative to the film. In case the detector is in the close-to-the-film vicinity, it fixes the total flux [see Fig. 10(c), dashed curve]. The interference pattern resulting from the existence of several homogeneous waves is quite noticeable in the far-field region in Fig. 11(b). The near-field structure may be understood in the same way as in the case of the $[r,0]$ resonance. For instance, when $\mathbf{E}$ is oriented along $\mathbf{g}_1+\mathbf{g}_2$, the intensity distribution on the quartz side for strictly normal incidence is proportional to $|\mathbf{E}^+|^2 \sim \sin^2[\mathbf{k}_{(1,1)t}\cdot\mathbf{r}]=\sin^2[(\mathbf{g}_1+\mathbf{g}_2)\cdot\mathbf{r}]$ [see the right-hand part of Fig. 11(a)]. When $\mathbf{E}$ is oriented with respect to $\mathbf{g}_1+\mathbf{g}_2$ at $\psi=\pi/4$, the near-field structure is formed by the interference of the eigenmode for $\sin[(\mathbf{g}_1+\mathbf{g}_2)\cdot\mathbf{r}]$ and the eigenmode for $\sin[(\mathbf{g}_1-\mathbf{g}_2)\cdot\mathbf{r}]$, so that the field at the interface takes the form $|\mathbf{E}^+|^2 \sim \{\sin[(\mathbf{g}_1+\mathbf{g}_2)\cdot\mathbf{r}]+\sin[(\mathbf{g}_1-\mathbf{g}_2)\cdot\mathbf{r}]\}^2$. This agrees with the left-hand part of Fig. 11(a). It is interesting to note that the field intensity is increased additionally in the regions where the inclusions are located.

D. $[1,0]_-$ resonance

It should be pointed out that SB SPP resonances pertinent to the superstrate face provide strong nonzeroth-order ELT on condition that $\varepsilon_- < \varepsilon_+$. It is clear from the geometrical reasons. Since the moduli of the wave vectors in the superstrate media are less than those of the substrate media, the metal-superstrate SPP wave vector ($k_{SPP}^- \simeq k\sqrt{\varepsilon_-}$) corresponds to the propagating wave in the substrate media. This enables SPP leakage without scattering via the modulation. Another feature of superstrate resonances is far deeper minima in the zeroth-order reflectance as compared to the resonance on the substrate face. This is because the zeroth-order reflectance is strongly dependent on the efficiency of SPP excitation. The incident light excites SPP on the superstrate face directly via the modulation, while for excitation on the substrate face, the amplitude of the light decreases prior to the excitation caused by the tunneling through the film (thereby making the excitation process less effective).

Let us discuss the SB metal-air $[1,0]_-$ SPP resonance that is consistent with the transmittance (reflectance) maximum (minimum) at $\lambda \simeq 0.92$ μm in Fig. 5. The enlarged fragments of the wavelength-dependent zeroth- and nonzeroth-order transmittances are shown in Fig. 12(a). While the zeroth-order transmittance profile is similar to that relating to the $[1,0]_+$ resonance [their maximal amplitudes are almost equal, being of order $\tau_{\mathcal{O}} \sim \exp(-2\Phi')$], the reflectance has considerably deeper minima [cf. Figs. 12(a) and 7(c)], in accordance with the above-mentioned general property of superstrate resonances. The amplitudes of the nonzeroth-order outgoing transmitted waves exceed significantly the zeroth-order amplitude [compare the solid curve for $\tau_{\mathcal{O}}$ and the dotted curve for $\tau_{[1,0]}$ in Fig. 12(a)] since their amplitudes are of order $\tau_{[1,0]} \sim \xi_{\mathcal{O}}'^{-1} \exp(-2\Phi')$. The latter statement follows from Eq. (B1). This estimation is quite universal and coincides with that made using Eq. (24) for the simplest resonance. The enhanced nonzeroth-order transmission may be used to develop the light splitters, since the waves propagate at an angle $\arccos(\beta_{r|+}\sqrt{\varepsilon_+})$ relative to the z axis. The unique feature of such a splitter is that all the four nonzeroth-order waves are linearly polarized. Their polarization coincides with that of SPPs excited.[33]

Note that not only $[1,0]$ diffraction orders are responsible for the nonzeroth-order ELT. As seen in Fig. 12(b), the diffraction orders $[1,1]$ correspond to the propagating waves in the quartz substrate as well. The resonance scattering contributes to these amplitudes so that they are proportional to $\tilde{\xi}_{[1,0]}^2$. Their intensities have been taken into account when calculating the total transmitted energy flux shown by the dashed line in Fig. 12(a).

It has to be stated that the transmittance behavior with respect to the polarization of the incident-wave variation, in the vicinity of $[1,0]_-$ resonance, is similar to that in the vicinity of $[1,0]_+$ resonance. This is described in Sec. III A

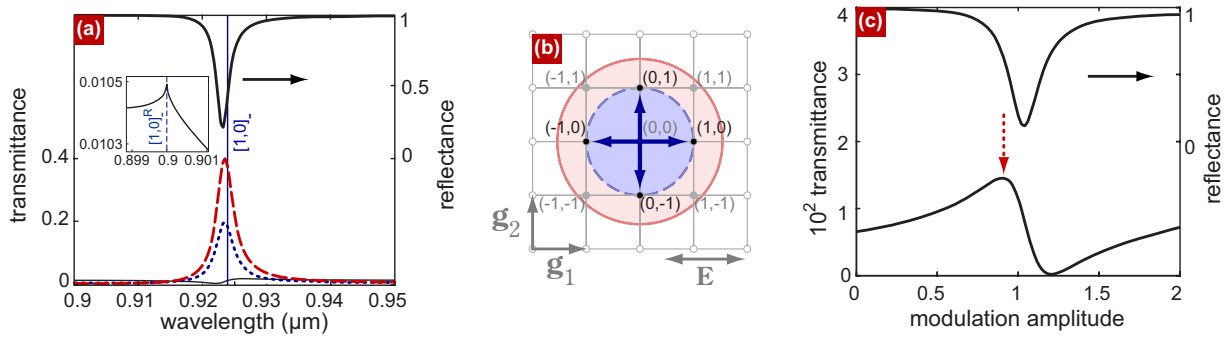

FIG. 12. (Color online) In (a), the wavelength dependence for the zeroth-order transmittance $\tau_{\mathcal{O}}$ and reflectance $\rho_{\mathcal{O}}$ (solid curves) along with the nonzeroth-order transmittance $\tau_{(\pm 1,0)}$ (dotted curve) and total transmittance τ_{tot} (dashed curve) are shown for the $[1,0]_-$ resonance on silver C_{4v} array of inclusions, $\mathbf{E}\|\mathbf{g}_1$, $\theta=0$. In the inset, the Rayleigh anomaly is shown. (b) The reciprocal grating [compare with Figs. 7(b) and 10(b)]. (c) The dependence of $\tau_{\mathcal{O}}$ and $\rho_{\mathcal{O}}$ on the modulation amplitude, $w=|(\xi_f-\xi_i)/\xi_f|$. The parameters of the array are the same as in Fig. 5.

[cf. the dashed square regions of λ-θ and the upper solid square regions in Fig. 6]. The near-field distribution in the X-Y plane is likewise equivalent to that corresponding to the $[1,0]_+$ resonance, but now the field is localized at the air-metal interface. This is clearly seen in Fig. 13(b). Note that the far-field structure has the form of the interference pattern both in the air and in the quartz half-spaces. The pattern in the air superstrate is due to the interference between incident and reflected zeroth-order waves: as seen in Fig. 12(a), the reflectance is of order of 20% in the resonance. The pattern in the quartz substrate results from the interference between the transmitted zeroth-order and nonzeroth-order waves.

Let us illustrate the dependence of the zeroth- and nonzeroth-order transmittance on the modulation amplitude. The transmittance (reflectance) has the well-defined maximum at $\xi_i \simeq 2\xi_f$, where $|\tilde{\xi}_{[1,0]}| \simeq 0.6\sqrt{\xi'_{\mathcal{O}}} \sim \sqrt{\xi'_{\mathcal{O}}}$ [see Fig. 12(c)]. So, as expected, this value of the modulation amplitude exactly provides for the resonance harmonic optimal magnitude, [see discussion below Eq. (30)] and, therefore, leads to the optimal transmittance.

E. Double-boundary SPP

DB SPPs for nonsymmetrically surrounded film exist under a specific relation between angle of incidence, wavelength, structure spacing, and dielectric permittivities of the surrounding media.[32] For instance, given strictly normal incidence, the excitation of four resonance waves in the superstrate ($\tau=+$) with multi-indexes $[r_+,0]$ and four resonance waves in the substrate ($\tau=-$) with multi-indexes $[r_-,0]$ may occur if $K_+/K_-=r_+/r_-$. We do not consider this specific set of parameters in the present paper, but study DB SPPs in a symmetrically surrounded film below.

IV. DB SPP RESONANCES IN THE SYMMETRICALLY SURROUNDED FILM

As far as we know, the earliest observations of the ELT through hole arrays due to the DB SPP excitation were described in Refs. 8 and 9. Moreover, in Ref. 8 the array was formed in the metal film surrounded by quartz from one face

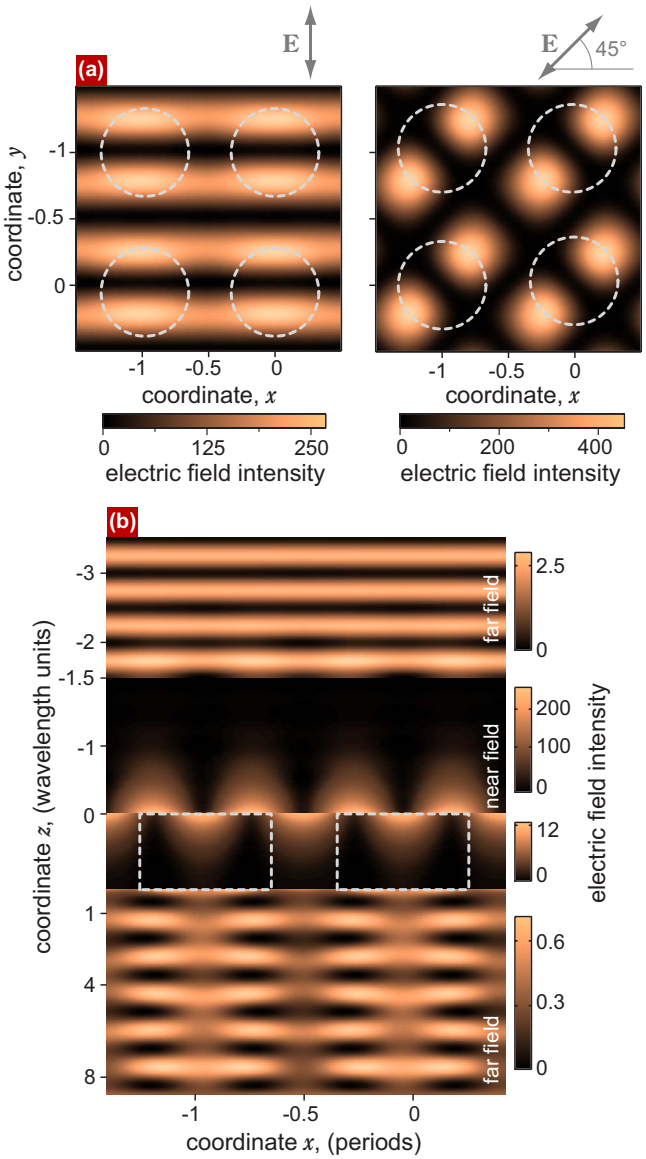

FIG. 13. (Color online) The intensity distribution is given for the $[1,0]_-$ SPP resonance at $\lambda=0.9234$ μm, $\theta=0$. The parameters of the array are the same as in Fig. 5.

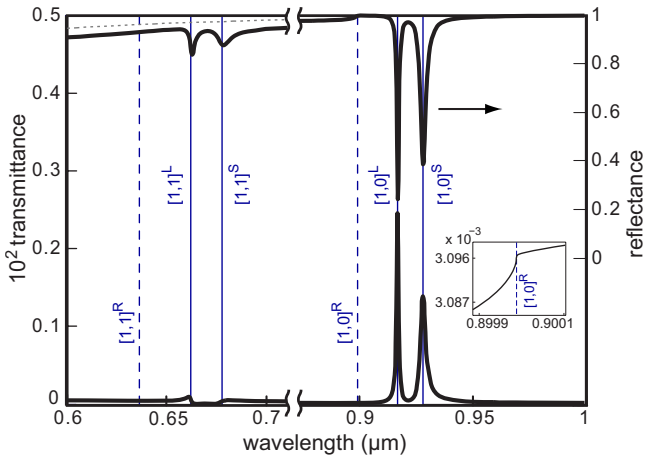

FIG. 14. (Color online) Wavelength-dependent transmittance and reflectance for strictly normal incidence onto the symmetrically surrounded (by air) silver film. The periodical array possesses C_{4v} symmetry, i.e., $\rho_1=\rho_2=\rho=0.9$ μm, $a/\rho=1/3$. $\mathbf{E}$ is parallel to $\mathbf{g}_1$ (to the x axis, see Fig. 1). The impedance of inclusions ξ_i is assumed to be $\xi_i=2\xi_f$. The film thickness is equal to 2.75 skin depths. The transmittance and reflectance for the unmodulated film are shown by dotted lines. Vertical solid (dashed) lines indicate the wavelengths for SPPs at unmodulated boundaries (Rayleigh points), one of them being shown in the inset.

and by a liquid with a close-to-quartz dielectric constant from the other face, while Ref. 9 deals with a freestanding film. In the above experiments, the wave vectors at the opposite interfaces were matched to excite a DB SPP. This led to a considerable increase of the ELT efficiency in the zeroth diffraction order as compared to the SB SPP excitation for a nonsymmetrically surrounded film.

Two SPP modes are known to exist in the nonmodulated symmetrically surrounded metal film (see Sec. II). One of them, i.e., a LR mode, is characterized by the nonsymmetric surface charge distribution, and a higher frequency and Q factor as compared to the other, a SR mode. It is interesting that a similar situation is inherent to the mechanical system of two coupled damping oscillators, which is nothing else but a classical analog of coupled SPPs in the film (see Appendix A). If the modulation is not too high, LR and SR modes undergo shifting and widening, but remain well separated from one another. This is not exactly what is observed in the experiments using subwavelength hole arrays. The modulation amplitude of the arrays is too high to clearly see the difference between LR and SR modes.

The transmittance spectra of a symmetrically surrounded film are shown in Fig. 14. One can observe the four peaks: the first pair is 0.663 μm, 0.683 μm in the vicinity of $[1,1]^{S,L}$ DB SPP resonance, and the second one is 0.918 μm, 0.929 μm in the vicinity of $[1,0]^{S,L}$ DB SPP resonance. Indexes S and L refer to LR and SR modes. In Figs. 15(a)–15(c) and 15(e), the transmittance spectra are shown as functions of the wavelength and/or energy and the incident angle for different polarizations of the incident wave. In Figs. 15(d) and 15(f), the resonance curves are shown by solid lines.

Consider the deviations from the normal incidence. In Figs. 15(a)–15(c), the special symmetry is depicted, that is, the incident plane is oriented relative to $\mathbf{g}_1$ at 0 and $\pi/4$. This corresponds to the coincidence of the resonance curves [see discussion below formula (18)], which is seen in the vicinity of the [1,0] resonance shown by square regions in Fig. 15. In Figs. 15(a)–15(c), these regions contain two to six resonance features [respectively, the highlighted regions in Figs. 15(d) and 15(f) contain two to six resonance curves]. On the contrary, in Fig. 15(e) the transmittance contour plot is shown for nonspecific geometry, and therefore, eight features (or eight curves) belong to each vicinity according to fourfold DB SPP.

Note the two features in Fig. 14. Firstly, the widths of resonance peaks (dips) are less for LR modes than for SR modes. This is due to the higher Q factor of the LR mode as compared with that of the SR mode, which can be easily explained in terms of the field structure of SPP modes in the metal. The z dependence of the electric field tangential component for LR and SR eigenmodes is defined by Eq. (35). Since the amplitude of the tangential component of the electric field is higher than the z component within the film, vector $\bar{\mathbf{E}}_t$ makes the principal contribution to the loss power P so that

$$\mathcal{P} \sim \int \varepsilon'' |\bar{\mathbf{E}}|^2 dv \sim \int_0^d |\bar{\mathbf{E}}_t|^2 dz, \tag{42}$$

In view of Eq. (35), one can see that the Ohmic losses of the SR mode are higher than those of LR mode, $P_s/P_l \sim (\sinh \Phi' + \Phi')/(\sinh \Phi' - \Phi') > 1$, which leads to the higher Q factor of the LR mode as compared with that of the SR mode.

Secondly, the resonance peaks for the LR and SR modes are strongly dependent on the exponential index appearing in the field approximation inside the film. In other words, assuming $\tilde{k}$ in Eq. (4) to be complex and taking into account both real and imaginary parts of the impedance of the conductor in Eq. (4), the transmittance maxima (reflectance minima) for the LR mode are higher (deeper) than those for the SR mode, and vice versa if dissipation losses are neglected. As was indicated in the experimental paper,[65] where plasmons were dealt with in the symmetrically surrounded corrugated silver film, "this process has a complex distance (film thickness) dependence." That is, "for thin silver films (<30 nm), the symmetric coupled SPP is strong but extremely sharp, whereas the antisymmetric SPP is broad but weak. As the silver thickness increases, the symmetric mode weakens and broadens, whereas the antisymmetric mode sharpens and intensifies." Thus, in our view, the discussed question of the resonance peaks for LR and SR modes needs further careful examination.

A. [1,0] resonance

Now, consider the [1,0] DB fourfold SPP resonance for strictly normal incidence. The enlarged fragment of Fig. 14 in the vicinity of the peaks is shown in Fig. 16(a). The LR and SR resonances are blueshifted as compared with the wavelengths for nonmodulated film SPPs marked by the vertical lines. Similar to the SB SPP resonance, the amplitudes

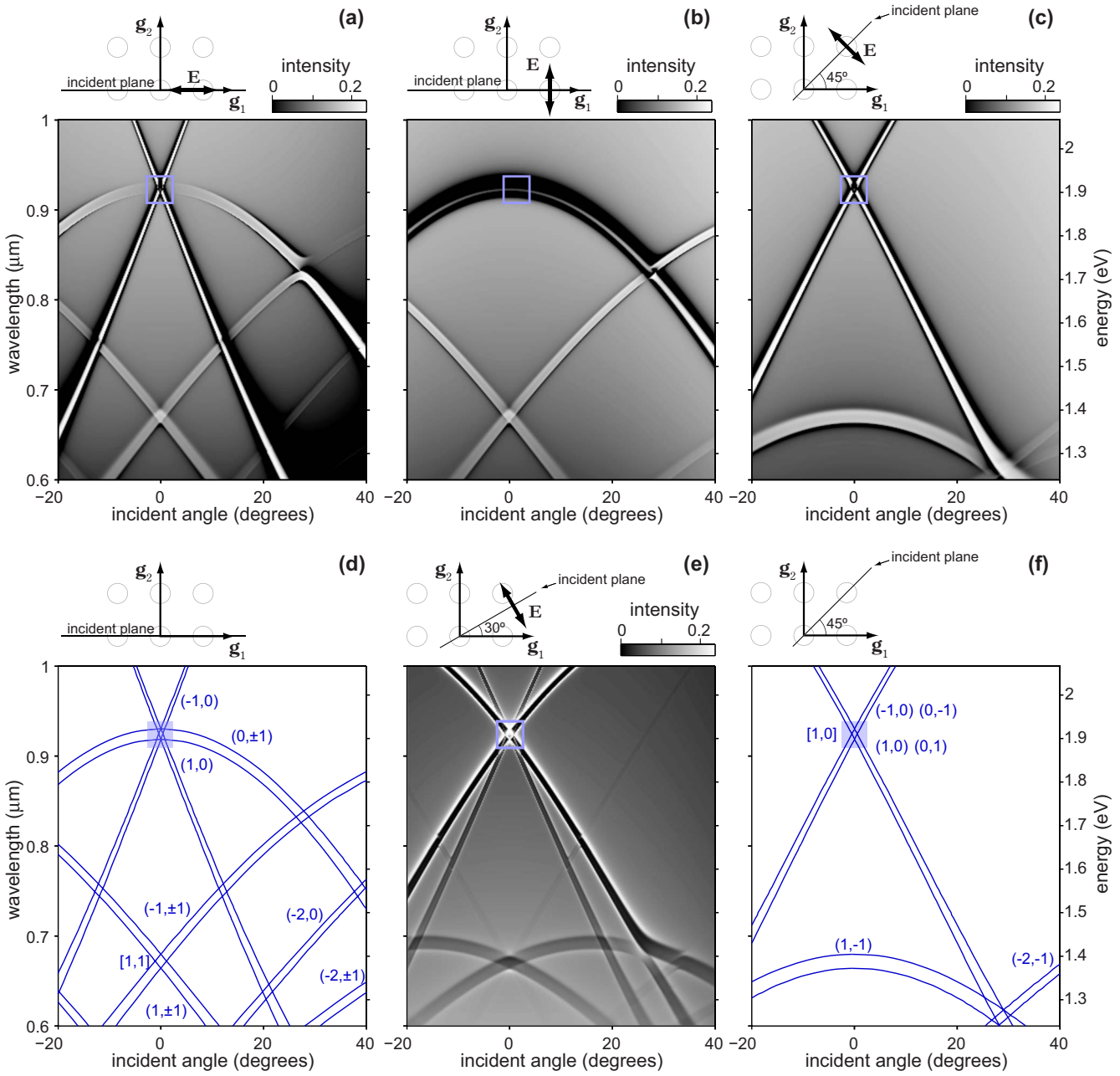

FIG. 15. (Color online) Transmittance as a function of the wavelength (energy) and the incident angle for different polarizations of the incident wave and different orientations of the incident plane. The parameters of the array and the film are the same as in Fig. 14. (d) and (f) show the resonance curves [see Eq. (18)]. Squares indicate the vicinity of the [1, 0] resonance that we consider in detail.

of the resonance waves are proportional to $\tilde{\xi}_{[10]}$, and the resonance contribution to the amplitude of the only propagating zeroth-order wave is proportional to $|\tilde{\xi}_{[10]}|^2$.

For a SDB resonance, the transmittance and reflectance have two extrema. This results from the excitation of LR and SR SPPs having the dispersion relations which coincide with the zeros of denominators $\Delta_{[1,0]}$ in Eqs. (29) and (30) (and Appendix B). The peak value of the transmittance for optimal modulation amplitude is estimated as $\tau_{\mathcal{O}} \sim \xi'^{-1}_{\mathcal{O}} \exp(-\Phi')$, which exceeds the transmittance through the unmodulated film by a factor of $\xi'^{-1}_{\mathcal{O}} \gg 1$.

The distance between the two extrema of the transmittance (reflectance) can be estimated by extracting the difference between the wavelengths of SR (LR) SPPs from the dispersion relations of Eq. (17). Using $\beta^{L,S}_{\mathcal{M}} = \varepsilon^{-1/2}\sqrt{1-(cq/\sqrt{\varepsilon}\omega^{L,S})^2}$ (where we have replaced $\mathbf{k}_{\mathcal{M}t}$ by the SPP wave vector $\mathbf{q}$), we find for the frequencies $\omega^{L,S} = cq/\sqrt{\varepsilon B^{L,S}}$, where for the LR mode $B^L = 1 - \varepsilon\xi^2_{\mathcal{O}} \tanh^2(\Phi/2)$ and for the SR mode $B^S = 1 - \varepsilon\xi^2_{\mathcal{O}} \coth^2(\Phi/2)$. We have $(\lambda^S - \lambda^L)/\lambda \sim |\xi''_{\mathcal{O}}|^2 \exp(-\Phi')$ for the relative difference between the wavelengths, where λ is of order of λ^S, λ^L. The modulation contributes additionally to

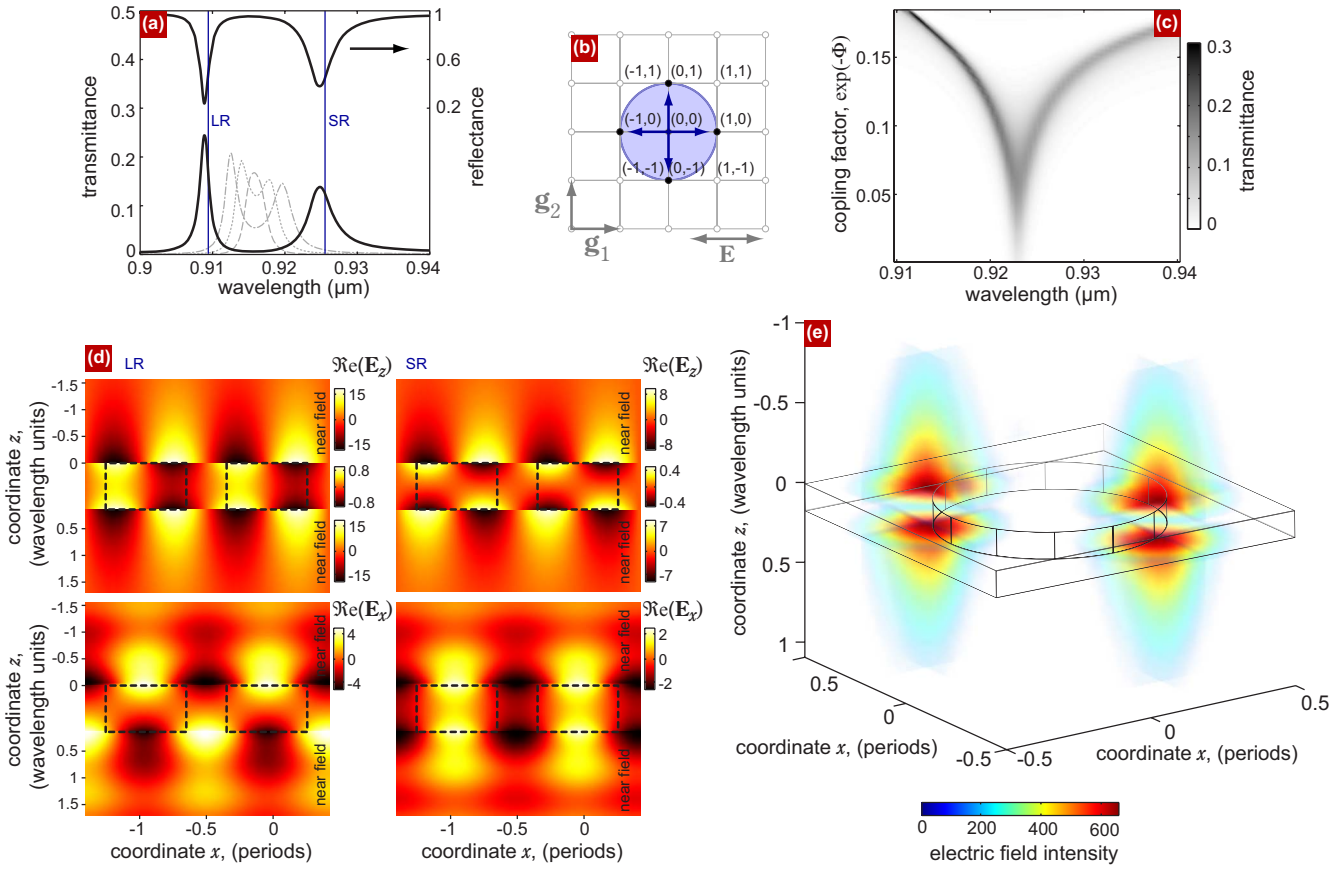

FIG. 16. (Color online) (a) The dependence of the zeroth-order transmittance $\tau_{\mathcal{O}}$ and reflectance $\rho_{\mathcal{O}}$ on the wavelength for the [1, 0] resonance on the silver array of inclusions (with symmetry C_{4v}), $\mathbf{E}\|\mathbf{g}_1$, $\theta=0$. (b) The reciprocal grating [compare with Figs. 7(b), 10(b), and 12(b)]. (c) The dependence of $\tau_{\mathcal{O}}$ on the wavelength and film thickness for $\theta=0$. [(d) and (e)] The distribution of tangential and normal components of the electric field at $\lambda=0.918$ μm (for the LR mode) and $\lambda=0.9285$ μm (for the SR mode), $\theta=0$. The inclusions in (d) are shown by the dashed lines. The parameters of the array are the same as in Fig. 14.

this difference, and this contribution can be found from the dispersion relation $\Delta_{\mathcal{R}}=0$ [Eq. (27)] (see Ref. 32). As the film thickness increases, the distance between λ^S and λ^L decreases [see Figs. 16(a) and 16(c)]. When the resonance width, $\Delta\lambda/\lambda\sim|\xi''_{\mathcal{O}}|\xi'_{\mathcal{O}}$, assumes the value of order of the splitting between the LR and SR modes, $\Delta\lambda\sim\lambda^S-\lambda^L$ [which occurs for film thickness $\Phi'\gtrsim\ln(|\xi''_{\mathcal{O}}|\xi'^{-1}_{\mathcal{O}})$], the two maxima of the two-humped resonance curve become indistinguishable.

The near-field distribution for LR and SR SPPs is shown in Figs. 16(d) and 16(e). One can see that the LR (SR) mode is antisymmetric (symmetric) with respect to the tangential component of the electric field and the surface charge distribution (the surface charge sign coincides with the sign of the product n_zE_z, where n_z is the z component of the surface normal vector directed out of the metal).

V. CONCLUSIONS

We have performed an analytical treatment of the resonance optical properties of 2D periodically modulated optically thick metal films. Explicit analytical expressions for transformation coefficients related to any diffraction order have been derived. In studying the complicated multiple resonances, we have ascertained that most of the physical properties of ELT may be thoroughly understood in terms of the simplest example of a solitary resonance (when a SPP is excited in a single diffraction order). We have examined and explained not only the amplitude and polarization dependences of the transmittance and reflectance on the parameters (such as angle of incidence, wavelength, tilting angle, film thickness, etc.) but also the field structure of the diffracted light. We have shown that according to the conception of interface SPPs excitation, the polarization dependences of the light diffracted by the periodical array may be adequately described. We have made a comparison between our theoretical calculations and recent experiments, thus having found excellent agreement. We have shown that it is difficult to make a distinction between the resonance features that are related to the excitation of the long-range and short-range SPP modes for hole arrays (which are, in most cases, used for the experimental study of ELT) because the radiative broadening is dominant over the splitting between these modes for relatively thick films. In this sense, weak-modulation structures (say, the periodical arrays of metal nanoparticles immersed into a metal film, corrugated shallow diffraction gratings) are more preferable. Moreover, the effi-

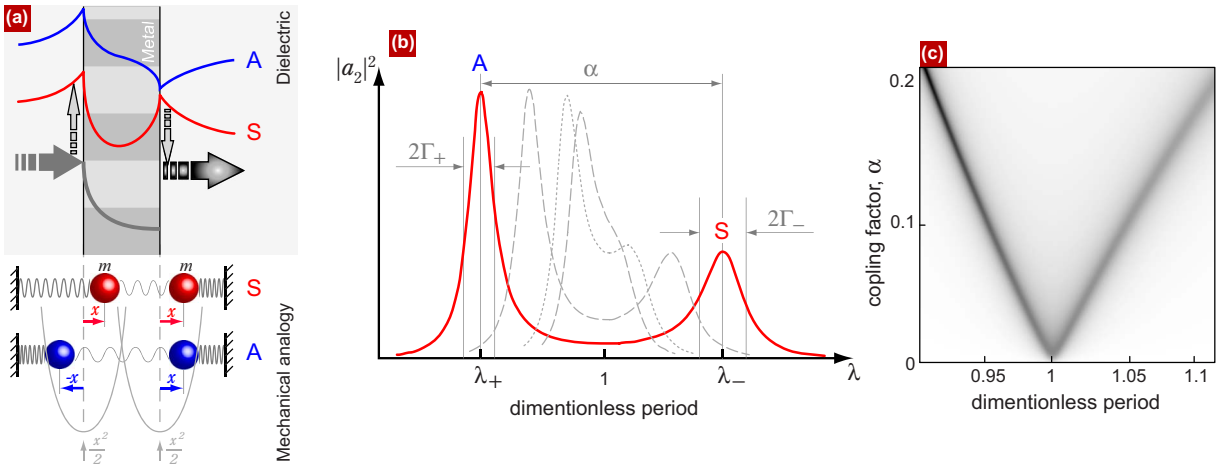

FIG. 17. (Color online) (a) The geometry of the diffraction problem and the mechanical analogy. (b) The dependence of "free" oscillator amplitude on the period $1/\Omega$. The coupling parameter and the damping are α=0.05, 0.03, 0.015, and 0.01 for the solid, dash-dotted, dotted, and dashed curves, respectively, and Γ_1=0.004 and Γ_2=0.001 are for all curves. (c) The "free" oscillator amplitude as a function of period $1/\Omega$ and coupling parameter α.

ciency of SPP excitation may be much higher for the structures with weak modulation as compared to the structures with holes being included. This is due to the existence of the optimal modulation amplitude. It has been demonstrated that in some cases the energy flux of nonzeroth diffraction orders exceeds that of zeroth-order. This can have a strong impact on the results of experimental measurements.

A highly instructive analogy has been drawn between the ELT effect and the motion of two weakly coupled classical oscillators driven by the monochromatic force.

ACKNOWLEDGMENT

The authors acknowledge financial support from the INTAS YS Grants Nos. Nr 05-109-5206 and Nr 05-109-5182.

APPENDIX A: TWO COUPLED DAMPING OSCILLATORS

The enhanced transparency and other resonant properties of the periodically modulated metal film can be described by analogy with a simple mechanical system consisting of two weakly coupled harmonic oscillators under the action of the harmonic force applied to one of them [see Fig. 17(a)]. The second oscillator amplitude is strongly dependent on the frequency of the force applied to the first oscillator and can reach values of order of the first uncoupled oscillator amplitude. We will concentrate on the system of two identical oscillators which is similar to the ELT through symmetrically surrounded film. Lagrangian of this system is

$$\mathcal{L} = \frac{1}{2}(\dot{x}_1^2 + \dot{x}_2^2) - \frac{1}{2}(x_1^2 + x_2^2) + \alpha x_1 x_2 + F_1(t)x_1 + F_2(t)x_2, \tag{A1}$$

where dots denote time derivatives, the term $\alpha x_1 x_2$ is responsible for weak coupling, $\alpha \ll 1$, and the two last terms are for the forces acting on the oscillators. Adding to the Lagrangian $-k(x_1^2+x_2^2)/2$, we arrive at the two masses linked by a string with elasticity coefficient k. The dimensionality of the variables is such that the unperturbed frequency is equal to unity. The losses are taken into account by the dissipative function[66]

$$\mathcal{F} = \mu_1(\dot{x}_1^2 + \dot{x}_2^2) + 2\mu_2 \dot{x}_1 \dot{x}_2, \tag{A2}$$

where $\mu_1 \geqslant |\mu_2| \geqslant 0$ (non-negativeness of $\mathcal{F}$). Below, the dissipation is supposed to be small, $|\mu_{1,2}| \ll 1$. Then, the equations of motion are written as

$$\frac{d}{dt}\frac{\partial \mathcal{L}}{\partial \dot{x}_i} = \frac{\partial \mathcal{L}}{\partial x_i} - \frac{\partial \mathcal{F}}{\partial \dot{x}_i}, \quad i = 1,2. \tag{A3}$$

In normal coordinates, $X_\mp = (x_1 \pm x_2)/\sqrt{2}$ for the inphase (X_-) and antiphase (X_+) oscillations (symmetric and antisymmetric with respect to transposition $1 \rightleftarrows 2$ modes), we split the system (A3),

$$\ddot{X}_\mp + (1 \mp \alpha)X_\mp + 2(\mu_1 \pm \mu_2)\dot{X}_\mp = F_\mp, \tag{A4}$$

where $F_\mp = (F_1 \pm F_2)/\sqrt{2}$.

The solution of the corresponding homogeneous system is

$$X_\pm = A_\pm \exp(-i\Omega_\pm t), \tag{A5}$$

where the complex eigenfrequencies are $\Omega_\mp$ and $-\Omega_\mp^*$ ($\mathrm{Re}\,\Omega_\mp > 0$, $\mathrm{Im}\,\Omega_\mp \leqslant 0$),

$$\Omega_\mp = -i(\mu_1 \pm \mu_2) + \sqrt{1 \mp \alpha - (\mu_1 \pm \mu_2)^2}$$
$$\simeq 1 \mp \frac{\alpha}{2} - \frac{(\mu_1 \pm \mu_2)^2}{2} - i(\mu_1 \pm \mu_2). \tag{A6}$$

The eigenfrequency of the inphase (symmetric) mode is lower than that for antiphase (antisymmetric) one, $\mathrm{Re}\,\Omega_- < \mathrm{Re}\,\Omega_+$ if the damping is small, $(\mu_1 \pm \mu_2)^2 \ll \alpha$. This is in compliance with the modes of the symmetrically sandwiched film. Specifically, the eigenfrequency of the LR (antisymmetric) SPP is lower than that for the SR (symmetric) one (see

discussions in Sec. IV A). The decrement $\Gamma_{\mp} \simeq \mu_1 \pm \mu_2$ is, in turn, higher (lower) for $\mu_2 > 0$ ($\mu_2 < 0$). Note that the case with $\mu_2 > 0$ holds for different active losses for symmetric and antisymmetric SPP modes. This difference results from the high-frequency mode having a lower mean value of the electric field in the film and, hence, lower losses and a higher Q factor.

The particular solution of the dynamic equations (A4) for harmonic driving forces being applied, $F_{1,2}=f_{1,2}\exp(-i\Omega t)$, is

$$X_{\pm}(t) = A_{\pm}(\Omega)\exp(-i\Omega t), \quad A_{\pm} = f_{\pm}/\mathcal{D}_{\pm}, \tag{A7}$$

where $f_{\pm}=(f_1 \mp f_2)/\sqrt{2}$ and

$$\mathcal{D}_{\pm} = \mathcal{D}_{\pm}(\Omega) = -(\Omega - \Omega_{\pm})(\Omega + \Omega_{\pm}^{*}). \tag{A8}$$

Thus, displacements of the forced oscillations are $x_i(t) = a_i(\Omega)\exp(-i\Omega t)$, $i=1,2$,

$$a_{1,2}(\Omega) = \frac{A_- \pm A_+}{\sqrt{2}} = \frac{f_1 + f_2}{2\mathcal{D}_-} \pm \frac{f_1 - f_2}{2\mathcal{D}_+}. \tag{A9}$$

Let the system be excited by a driving force applied to the first oscillator, $f_1=4$, $f_2=0$. This is analogous to the diffraction problem, in which only one wave is incident onto the metallic film face. If the dissipation is small, $(\mu_1 \pm \mu_2)^2 \ll \alpha$, then two pronounced maximal magnitudes of $a_{1,2}$ arise in the neighborhood of the frequencies $\Omega=\Omega'_{\mp}$, where $a_{1,2}(\Omega'_-) \simeq 2/\mathcal{D}_-(\Omega'_-) \simeq i/\Gamma_-$, $a_{1,2}(\Omega'_+) \simeq \pm 2/\mathcal{D}_+(\Omega'_+) \simeq \pm i/\Gamma_+$. The splitting of the resonance maxima is approximately α, and the high- (low-) frequency resonance widths are $\delta\Omega_{\pm}=2\Gamma_{\pm}$. As α decreases, the distance between resonance peaks diminishes, and for $\alpha \sim \Gamma_+ + \Gamma_-$ they overlap [see Figs. 17(b) and 17(c)]. The mechanical coupling factor α is similar to that arising in the EM problems: for the splitting of the SPP modes in the film, this factor is $\exp(-\Phi')$ [cf. Figs. 17(c) and 16(c)].

For $\mu_1=\mu_2=0$, the amplitude of the enforced oscillator vanishes at unperturbed eigenfrequency, $\Omega=1$. This well-known resonance damping effect (which is extensively used in shipbuilding) also highlights an analogy with the ELT problem, where Fano minima appear in the field amplitudes.

In a similar way, one can make an analogy for the nonsymmetrically sandwiched film. In this particular case, the mechanical system consists of two oscillators of different masses.

Thus, some physical properties of the ELT phenomena are sufficiently general. At least, the similarities to the simplest classical mechanical systems may be established.

APPENDIX B: TRANSFORMATION COEFFICIENTS FOR FOURFOLD RESONANCE IN CASES OF C_{2v} AND C_{4v} SYMMETRIES

In the case of C_{2v} symmetry which implies the following properties of modulation impedance,

$$\tilde{\xi}_{n_1,n_2} = \tilde{\xi}_{-n_1,n_2} = \tilde{\xi}_{n_1,-n_2} = \tilde{\xi}_{-n_1,-n_2},$$

the resonance matrix possesses the symmetry properties. The resonance TCs in the vicinity of normal incidence for the $[r,0]$ or $[r,0]_\tau$ resonance are related as $T^{\tau|-\sigma}_{r,0} = -T^{\tau|-\sigma}_{-r,0}$, $T^{\tau|-\sigma}_{0,r} = -T^{\tau|-\sigma}_{0,-r}$. This allows Eqs. (19) and (22) to be significantly simplified: the resonance 8×8 matrix can be reduced to a 2×2 matrix. Thus, the TCs are written as

$$T^{\tau|-\sigma}_{\mathcal{R}} = -\frac{2\tau\sigma\sqrt{\varepsilon_-}S^{\bar{\sigma}}_{\mathcal{R}\mathcal{O}}\tilde{\xi}_{\mathcal{R}}\beta^{(1+\sigma)/2}_{-|\mathcal{O}}}{\Delta_{\mathcal{R}}}[\tilde{\beta}_{\bar{\tau}|\mathcal{R}} - \Upsilon_{\mathcal{R}}(\cosh\Phi)^{\tau-1}] \times (\cosh\Phi)^{-(1+\tau)/2}, \tag{B1}$$

where $\mathcal{R}=(r,0)$ or $\mathcal{R}=(0,r)$,

$$\Delta_{\mathcal{R}} = \tilde{\beta}_{+|\mathcal{R}}\tilde{\beta}_{-|\mathcal{R}} - \Upsilon^2_{\mathcal{R}}\cosh^{-2}\Phi,$$

$$\tilde{\beta}_{\tau|\mathcal{R}} \equiv \beta_{\tau|\mathcal{R}}\tanh\Phi + \xi_{\mathcal{O}} + \tilde{\xi}_{2\mathcal{R}} + G^{\tau}_{\mathcal{R}},$$

$$\Upsilon_{\mathcal{R}} = \xi_{\mathcal{O}} + \tilde{\xi}_{2\mathcal{R}} + G^{+}_{\mathcal{R}} + G^{-}_{\mathcal{R}},$$

$$G^{\tau}_{\mathcal{R}} = -\sum_{\mathcal{N}} \frac{\tilde{\xi}_{\mathcal{R}-\mathcal{N}}(\tilde{\xi}_{\mathcal{N}-\mathcal{R}} + \tilde{\xi}_{\mathcal{N}+\mathcal{R}})}{\beta_{\tau|\mathcal{N}}}(C^2_{\mathcal{R}\mathcal{N}} + \varepsilon_\tau\beta^2_{\tau|\mathcal{N}}S^2_{\mathcal{R}\mathcal{N}}), \tag{B2}$$

$$T^{\tau|\sigma\sigma'}_{\mathcal{N}} = \delta_{\mathcal{N},\mathcal{O}}\delta_{\sigma,\sigma'}T^{\tau|\sigma}_{F} + A^{\tau}_{\mathcal{N}|\sigma}(\cosh\Phi)^{-(1+\tau)/2}\sum_{\mathcal{R}} \frac{\tilde{\xi}_{\mathcal{R}}S^{\bar{\sigma}}_{\mathcal{N}\mathcal{R}}S^{\overline{\sigma'}}_{\mathcal{R}\mathcal{O}}(\tilde{\xi}_{\mathcal{N}-\mathcal{R}} + \tilde{\xi}_{\mathcal{N}+\mathcal{R}})}{\Delta_{\mathcal{R}}} \times [\tilde{\beta}_{\bar{\tau}|\mathcal{R}} + (\tilde{\beta}_{\tau|\mathcal{R}} - \Upsilon_{\mathcal{R}})(\cosh\Phi)^{\tau-1}], \tag{B3}$$

where $A^{\tau}_{\mathcal{N}|\sigma} = 2\sigma'\tau^{(1-\sigma)/2}\varepsilon^{(1+\sigma)/4}_{\tau}\varepsilon^{(1+\sigma')/4}_{-}\beta^{(1+\sigma')/2}_{-|\mathcal{O}}\beta^{(\sigma-1)/2}_{\tau|\mathcal{N}}$. If the modulation has C_{4v} symmetry, the zeroth-order TCs permit additional simplifications,

$$T^{\tau|\sigma\sigma}_{\mathcal{O}} = T^{\tau|\sigma}_{F} + \frac{2\sigma A^{\tau}_{\mathcal{O}|\sigma}\tilde{\xi}^2_{\mathcal{R}}}{\Delta_{\mathcal{R}}}[\tilde{\beta}_{\bar{\tau}|\mathcal{R}} + (\tilde{\beta}_{\tau|\mathcal{R}} - \Upsilon_{[r,0]})(\cosh\Phi)^{\tau-1}] \times (\cosh\Phi)^{-(1+\tau)/2}, \quad T^{\tau|\sigma\bar{\sigma}}_{\mathcal{O}} = 0. \tag{B4}$$

Note that the zeroth-order TCs are diagonal in polarization, i.e., the polarization of zeroth-order reflected and/or transmitted wave is the same as that of the incident wave.

*ak_04@rambler.ru
†nesterovml@web.de
‡alexeynik@rambler.ru

[1] H. Raether, *Surface Plasmons* (Springer-Verlag, New York, 1988).
[2] V. M. Agranovich and D. L. Mills, *Surface Polaritons* (Nauka, Moscow, 1985).
[3] A. V. Zayats, I. I. Smolyaninov, and A. A. Maradudin, Phys. Rep. **408**, 131 (2005).
[4] W. L. Barnes, A. Dereux, and T. W. Ebbesen, Nature (London) **424**, 824 (2003).
[5] T. W. Ebbesen, H. J. Lezec, H. F. Ghaemi, T. Thio, and P. A. Wolff, Nature (London) **391**, 667 (1998).
[6] H. F. Ghaemi, T. Thio, D. E. Grupp, T. W. Ebbesen, and H. J. Lezec, Phys. Rev. B **58**, 6779 (1998).
[7] H. A. Bethe, Phys. Rev. **66**, 163 (1944).
[8] A. Krishnan, T. Thio, T. J. Kim, H. J. Lezec, T. W. Ebbesen, P. A. Wolf, J. Pendry, L. Martin-Moreno, and F. J. García-Vidal, Opt. Commun. **200**, 1 (2001).
[9] L. Martín-Moreno, F. J. García-Vidal, H. J. Lezec, K. M. Pellerin, T. Thio, J. B. Pendry, and T. W. Ebbesen, Phys. Rev. Lett. **86**, 1114 (2001).
[10] J. Dintinger, S. Klein, F. Bustos, W. L. Barnes, and T. W. Ebbesen, Phys. Rev. B **71**, 035424 (2005).
[11] Y. Liu and S. Blair, Opt. Lett. **28**, 507 (2003).
[12] W. A. Murray, S. Astilean, and W. L. Barnes, Phys. Rev. B **69**, 165407 (2004).
[13] A. Degiron, H. J. Lezec, W. L. Barnes, and T. W. Ebbesen, Appl. Phys. Lett. **81**, 4327 (2002).
[14] S. C. Hohng, Y. C. Yoon, D. S. Kim, V. Malyarchuk, R. Müller, Ch. Lienau, J. W. Park, K. H. Yoo, J. Kim, H. Y. Ryu, and Q. H. Park, Appl. Phys. Lett. **81**, 3239 (2002).
[15] F. J. Garcia-Vidal, L. Martín-Moreno, and J. B. Pendry, J. Opt. A, Pure Appl. Opt. **7**, S97 (2005).
[16] M. Sarrazin, J.-P. Vigneron, and J.-M. Vigoureux, Phys. Rev. B **67**, 085415 (2003).
[17] E. Popov, M. Nevière, S. Enoch, and R. Reinisch, Phys. Rev. B **62**, 16100 (2000).
[18] R. Petit and M. Neviere, *Light Propagation in Periodic Media: Differential Theory and Design* (Dekker, New York, 2003).
[19] L. Salomon, F. Grillot, A. V. Zayats, and F. de Fornel, Phys. Rev. Lett. **86**, 1110 (2001).
[20] D. Gérard, L. Salomon, F. de Fornel, and A. V. Zayats, Opt. Express **12**, 3652 (2004).
[21] U. Schröter and D. Heitmann, Phys. Rev. B **60**, 4992 (1999).
[22] P. T. Worthing and W. L. Barnes, Appl. Phys. Lett. **79**, 3035 (2001).
[23] I. Arutsky, Y. Zao, and V. Kochergin, Opt. Lett. **25**, 595 (2000).
[24] N. Bonod, S. Enoch, L. Li, E. Popov, and M. Nevière, Opt. Express **11**, 428 (2003).
[25] S. A. Darmanyan and A. V. Zayats, Phys. Rev. B **67**, 035424 (2003).
[26] A. M. Dykhne, A. K. Sarychev, and V. M. Shalaev, Phys. Rev. B **67**, 195402 (2003).
[27] S. A. Darmanyan, M. Nevière, and A. V. Zayats, Phys. Rev. B **70**, 075103 (2004).
[28] Z. D. Genchev and D. G. Dosev, J. Exp. Theor. Phys. **99**, 1129 (2004).
[29] Yu. P. Bliokh, J. Felsteiner, and Y. Z. Slutsker, Phys. Rev. Lett. **95**, 165003 (2005).
[30] A. Benabbas, V. Halté, and J.-Y. Bigot, Opt. Express **13**, 8730 (2005).
[31] A. V. Kats and A. Yu. Nikitin, JETP Lett. **79**, 625 (2004).
[32] A. V. Kats and A. Yu. Nikitin, Phys. Rev. B **70**, 235412 (2004).
[33] A. V. Kats, M. L. Nesterov, and A. Yu. Nikitin, Phys. Rev. B **72**, 193405 (2005).
[34] S. Park, G. Lee, S. H. Song, C. H. Oh, and P. S. Kim, Opt. Lett. **28**, 1870 (2003).
[35] K. G. Lee and Q.-H. Park, Phys. Rev. Lett. **95**, 103902 (2005).
[36] G. Laurent, N. Félidj, S. Lau Truong, J. Aubard, G. Lévi, J. R. Krenn, A. Hohenau, A. Leitner, and F. R. Aussenegg, Nano Lett. **5**, 253 (2005).
[37] M. D. Malinsky, K. L. Kelly, G. C. Schatz, and R. P. V. Duyne, J. Am. Chem. Soc. **123**, 1471 (2001).
[38] Y. Xia and N. J. Halas, MRS Bull. **30**, 338 (2005).
[39] K. J. Klein Koerkamp, S. Enoch, F. B. Segerink, N. F. van Hulst, and L. Kuipers, Phys. Rev. Lett. **92**, 183901 (2004).
[40] A. Degiron and T. Ebbesen, J. Opt. A, Pure Appl. Opt. **7**, S90 (2005).
[41] K. L. van der Molen, K. J. Klein Koerkamp, S. Enoch, F. B. Segerink, N. F. van Hulst, and L. Kuipers, Phys. Rev. B **72**, 045421 (2005).
[42] Gang Sun and C. T. Chan, Phys. Rev. E **73**, 036613 (2006).
[43] T. A. Kelf, Y. Sugawara, R. M. Cole, J. J. Baumberg, M. E. Abdelsalam, S. Cintra, S. Mahajan, A. E. Russel, and P. N. Bartlett, Phys. Rev. B **74**, 245415 (2006).
[44] T. V. Teperik, V. V. Popov, F. Javier García de Abajo, M. Abdelsalam, P. N. Bartlett, T. A. Kelf, Y. Sugawara, and J. J. Baumberg, Opt. Express **14**, 1965 (2006).
[45] R. Gordon, A. G. Brolo, A. McKinnon, A. Rajora, B. Leathem, and K. L. Kavanagh, Phys. Rev. Lett. **92**, 037401 (2004).
[46] J. Elliott, I. I. Smolyaninov, N. I. Zheludev, and A. V. Zayats, Opt. Lett. **29**, 1414 (2004).
[47] E. Altewischer, C. Genet, M. P. van Exter, J. P. Woerdman, P. F. A. Alkemade, A. van Zuuk, and E. W. J. M. van der Drift, Opt. Lett. **30**, 90 (2005).
[48] C. Genet, E. Altewischer, M. P. van Exter, and J. P. Woerdman, Phys. Rev. B **71**, 033409 (2005).
[49] F. Miyamaru and M. Hangyo, Appl. Opt. **43**, 1412 (2004).
[50] S. A. Maier, Curr. Nanosci. **1**, 17 (2005).
[51] J. Homola, S. S. Yee, and Gunter Gauglitz, Sens. Actuators B **54**, 3 (1999).
[52] J. Homola, Anal. Bioanal. Chem. **377**, 528 (2003).
[53] P. V. Lambeck, Meas. Sci. Technol. **17**, R93 (2006).
[54] A. G. Schuchinsky, D. E. Zelenchuk, and A. M. Lerer, J. Opt. A, Pure Appl. Opt. **7**, S102 (2005).
[55] J. Saxler, J. G. Rivas, C. Janke, H. P. M. Pellemans, P. H. Bolívar, and H. Kurz, Phys. Rev. B **69**, 155427 (2004).
[56] For a modulated film, SB SPPs can be coupled by diffraction. Such DB dressed SPPs exist when the specific relations between permittivities of the dielectric media are satisfied. Formally, these relations result from the simultaneous vanishing of two determinants, $\|b_{\mathcal{M}}^{\tau\tau'|\sigma}\|$ and $\|b_{\mathcal{M}'}^{\tau\tau'|\sigma}\|$, with $\mathcal{M}' \neq \mathcal{M}$, and in calculating the matrix determinant $D_{\mathcal{M}\mathcal{M}'}^{\tau\tau'|\sigma\sigma''}$ (in the lowest order in the modulation), one has to take into account the products of the determinants of the diagonal-in-diffraction order submatrices $b_{\mathcal{M}''}^{\tau\tau'|\sigma}$ along with the terms corresponding to the submatrices $d_{\mathcal{M}\mathcal{M}'}^{\tau\tau'|\sigma\sigma'}$, $d_{\mathcal{M}'\mathcal{M}}^{\tau\tau'|\sigma\sigma'}$.
[57] F. Yang, J. R. Sambles, and G. W. Bradberry, Phys. Rev. B **44**,

5855 (1991).
[58] J. J. Burke, G. I. Stegeman, and T. Tamir, Phys. Rev. B **33**, 5186 (1986).
[59] Indeed, the resonance curves have the finite width due to the dissipative and radiative losses and, therefore, it is more appropriate to refer to the resonance vicinity, but not to the resonance point.
[60] A. V. Kats and A. Y. Nikitin, Proc. SPIE **5221**, 218 (2003); **5477**, 381 (2004).
[61] M. Kretschmann and A. A. Maradudin, Phys. Rev. B **66**, 245408 (2002).
[62] N. Fang, H. Lee, C. Sun, and X. Zhang, Science **308**, 534 (2005).
[63] In case of the periodicity formed by the surface relief corrugation, the situation changes radically: coupling does exist even when SPPs propagate perpendicular to one another.
[64] V. M. Zolotarev, V. N. Morozov, and E. V. Smirnova, *Optical Constants of Natural Media* (Chemistry, Leningrad, 1984).
[65] P. Andrew and W. L. Barnes, Science **306**, 1002 (2004).
[66] L. D. Landau and E. M. Lifshits, *Classical Mechanics* (Pergamon, Oxford, 1977).